MSc Thesis Biomedical Engineering

Decoding Motor Unit Firing Events During Walking: An Adaptive Approach Validated with Intramuscular Electromyography

B.J. van Dieren

Graduation Committee:

dr.ir. T. Heida

dr.ir. A. Gogeascoechea

dr. S.U. Yavüz

prof.dr.ir M. Sartori

March, 2025

Department of Biomedical Signals and Systems
Faculty of Electrical Engineering,
Mathematics and Computer Science

UNIVERSITY OF TWENTE.

CONTENTS

I Introduction 3

II Background 4
II-A EMG generation model . . . 4
II-B iEMG decomposition . . . 5
II-C HD-EMG . . . 5
II-D Blind source seperation . . . 5
II-E Evaluation of decomposition accuracy . . . 6
II-F Online Decomposition . . . 6
II-G Applications of Motor Unit Spike Trains . . . 7
II-H Dynamic conditions and adaptive algorithms . . . 7

III Methods 8
III-A Data Collection . . . 8
III-A.1 Participant preparation . . . 8
III-A.2 Motion analysis . . . 8
III-A.3 Experiment protocol . . . 9
III-A.4 Signal Processing . . . 9
III-B Offline Procedures . . . 9
III-B.1 Offline parameter estimation . . . 9
III-B.2 MU twitch properties estimation . . . 9
III-C Online procedures . . . 10
III-C.1 Adaptive decomposition . . . 10
III-C.2 Static decomposition . . . 10
III-C.3 MU-specific activation dynamics . . . 11
III-D Validation procedures . . . 11
III-D.1 iEMG template matching . . . 11
III-D.2 MU firing validation . . . 11
III-D.3 Using MU filters across trials . . . 11
III-D.4 MU-specific activation assessment . . . 11
III-D.5 Real-time assessment . . . 11

IV Results 12

V Discussion 12
V-A Adaptive Algorithm implementation . . . 12
V-A.1 Rationale . . . 12
V-A.2 Stability analysis . . . 13
V-B Static versus adaptive algorithms in changing MUAP shapes . . . 13
V-C Static versus adaptive algorithms across conditions . . . 15
V-D Computational time . . . 15
V-E Translation into MU specific activation patterns . . . 15
V-F Limitations and recommendations . . . 16

VI Conclusion 17

References 17

Appendices 19
-A Processing Pipeline . . . 19
-B Results Subject 1 . . . 21
-B.1 Using MU filters within a trial . . . 21
-B.2 Using MU filters across conditions/trials . . . 22
-C Unstable Decomposition . . . 23

Decoding Motor Unit Firing Events During Walking: An Adaptive Approach Validated with Intramuscular Electromyography

Abstract— **Motor unit decomposition from high-density surface electromyography (HD-EMG) provides insights into neural control of movement. However, variations in motor unit action potential (MUAP) shapes during dynamic conditions, such as walking, pose challenges for decomposition accuracy. This thesis presents an adaptive framework to address these challenges, focusing on the m. soleus in walking.**

The framework consists of: (1) an offline procedure to extract decomposition parameters from low-force isometric and walking trials, (2) an online-ready system applying these parameters in static and adaptive algorithms to estimate MU-specific activation dynamics, and (3) validation against intramuscular EMG (iEMG) benchmarks.

Results showed that static decomposition performed well at lower speeds (0.6 m/s), while the adaptive algorithm improved robustness in dynamic conditions for processing windows $\geq$ 200 ms. When train and test datasets were from different trials, the adaptive method significantly outperformed the static approach.

This adaptive approach enables real-time tracking of m. soleus motor unit activity, with applications in movement analysis, rehabilitation and human-machine interfacing. Future research should optimize parameters for muscles with greater MUAP variability and validate the method in impaired populations. Integrating adaptive decomposition with neuromusculoskeletal models could enhance joint torque estimation and real-time control of wearable robotics.

Significance: A conference proceeding containing preliminary results from an earlier draft of this thesis has been accepted and selected as a finalist for the Best Paper Award at Rehabweek 2025.

I. INTRODUCTION

Human movement is driven by interplay between neural commands and muscle fibers. The smallest functional unit responsible for force generation is the motor unit (MU), consisting of an alpha-motor neuron and the muscle fibers it innervates [1]. Gaining insight into the mechanisms underlying the functioning of motor units is crucial for understanding both normal and impaired motor function. [2]–[4]. The goal of this thesis is to improve the estimation of motor unit firing patterns under dynamic and real-world conditions. Decoding motor unit activity in these scenarios provides valuable insights into the underlying mechanisms of muscle function and contributes to the development of strategies for mobility restoration and rehabilitation in individuals with motor impairments.

When a MU is activated, it produces an action potential. This action potential travels from the dendrites along the cell to the axon, where the muscle fibers are activated. These muscle fiber action potentials (MFAPs) cause muscle fibers to contract, resulting in force production and movement. The total sum of all the MFAPs of the muscle fibers belonging to one motor unit is called the motor unit action potential (MUAP) [1], [5]. A visual representation of the MUAP can be seen in figure 1.A.

Traditional methods to record single motor unit activity involve intramuscular electromyography (iEMG) recordings using fine-wire or needle electrodes [6]. Template matching algorithms have been proposed as a method for decomposing iEMG signals, enabling full decomposition that provides insight into single motor unit behavior [7], [8]. This technique identifies surface motor unit action potentials (sMUAP) by detecting their characteristic shapes and amplitudes and classifies them into specific motor units based on these features. However, the main limitation of this technique is its inability to distinguish action potentials that overlap in time, often resulting in incomplete action potential trains [6].

In recent years, high-density electromyography (HD-EMG) has emerged as a technique that can non-invasively record temporal and spatial muscle activity on the skin's surface [9], [10], with an example of such a grid shown in figure 1.B. Combined with blind source separation (BSS), this approach enables the identification of motor unit (MU) discharge patterns in vivo without requiring *a priori* knowledge of MUAP shapes. Instead, it relies on the statistical properties of MU discharges and filter properties of sMUAPs [11], [12]. Several studies have demonstrated the potential of this technique to investigate common synaptic input in force generation [13], [14], explore the mechanisms underlying essential tremor [3], [15], and assess the effects of electrical stimulation on motor unit pools in individuals with incomplete spinal cord injury (SCI) [4]. Additionally, it has shown potential when combined with personalized musculoskeletal modeling for human-machine interfacing, offering promising applications in movement analysis and exoskeleton control [16], [17].

Although current BSS techniques have been extensively validated for isometric contractions, they assume stationary conditions [11], [18], making them suitable only for isometric or slow dynamic tasks. This limits their applicability to real-world dynamic scenarios like hand gestures or walking in which factors such as innervation zone and tendon shifts relative to the electrodes [19], [20], volume conduction changes, and joint angle variations [21] change sMUAP characteristics throughout movement. Even the MUAPs during consistent isometric contractions are prone to changes due to fatigue and changes in firing patterns over time [22]. Another big limitation of HD-EMG recordings is its susceptability to amplitude cancellation, which refers to the phenomenon where overlapping sMUAPs of opposite polarity partially or completely cancel each other out [23]. This effect poses

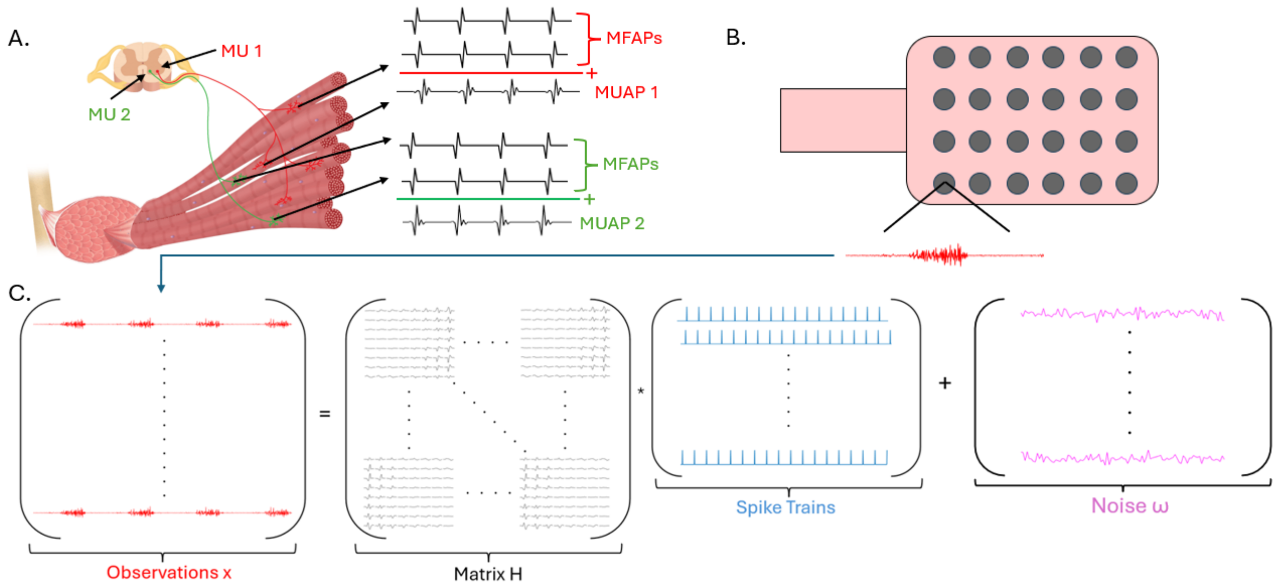

Fig. 1. A: Motor units (MU 1 in red, MU 2 in green) generate motor unit action potentials (MUAPs), which is the sum of individual muscle fiber action potentials (MFAPs). B: High-density EMG (HD-EMG) uses an electrode grid to record spatial and temporal muscle activity on the skins surface. C: Extended observations, i.e. surface EMG signals, (x) are modeled as the convolution of mixing matrix H, which contains the MUAPs and their delayed versions for all motor units and across all channels, and the extended motor unit spike trains, with added extended noise (ω)

significant challenges when trying to analyzing low-threshold MUs during high-force activities, such as walking, because the recruitment and elevated firing rates of high-threshold MUs amplify the likelihood and severity of amplitude cancellation.

These limitations restrict the use of motor unit decomposition in movement analysis and exoskeleton control for both healthy and impaired individuals, as well as improvement of neuro-rehabilitation techniques such spinal stimulators, and neuroprosthetics in impaired individuals [2], [4]. Addressing these limitations would enhance the understanding of neuromuscular control during dynamic tasks and pave the way for targeted interventions in motor disorders and improved exoskeleton control.

To address amplitude cancellation, previous work already proposed a decoding algorithm that is capable of identifying the MU firing events from a wide range of MU types, by extracting both low-force motor units from quasi-isometric contractions and high-force motor units in walking data [16]. This study focused on MUAPs from the m. soleus, which undergoes minimal fiber length changes during the push-off phase, minimizing the MUAP shape changes during activation. [24], [25]. However, this study used a static decomposition approach, which does not cover the non-stationairy nature of sMUAPs during dynamic conditions [16]. Another big limitation was the lack of validation at a motor unit level with iEMG benchmarks, as this is a reliable approach for validating decomposition accuracy, because it is a direct and high-selectivity method to identify individual motor unit spike trains (Section II-B).

To overcome these limitations, recent advancements proposed adaptive approaches in which filters are adapted in real-time to changing measurement conditions. In these algorithms, decomposition parameters are updated based on new data to adapt to changes in sMUAP shapes over time. However, current implementations have only tried this approach in slow dynamic contractions [26], [27] or isometric conditions [28] making them less relevant in decoding MU activity in dynamic movements such as walking. Also, these models are either validated on hybrid data, in which simulated and experimental HD-EMG recordings are used, or with signal-based metrics without acquiring iEMG benchmarks for comparison. Only Yeung et al. [28] did acquire iEMG benchmarks; however, their study was limited to isometric trials performed at varying force levels and joint angles.

Therefore, the aim of this thesis was to extend the methodology to address variations in MUAP shapes during locomotion by proposing an adaptive algorithm and validating its accuracy using intramuscular EMG (iEMG) as the benchmark for decomposition. This thesis (1) applies offline-initialized filters in an adaptive online framework to estimate MU activity, (2) validates this MU activity against an iEMG benchmark to obtain a conservative estimation of accuracy and (3) combines the MU spike trains in combination with twitch properties to determine overall muscle activation patterns [16]. This approach enables more accurate estimates of MU firing patterns in dynamic contractions, which has the potential to transform the development of assistive devices. Through real-time adaptability and intergration with personalised muscoloskeletal models this will allow for a personalized and effective rehabilitation experience for every user.

II. Background

A. EMG generation model

The generation model of multi-channel surface EMG signals can be described as a convolutive mixture of impulses with their corresponding sMUAPs. These sMUAPs have a finite duration [11] and therefore the mixing process can be presented as:

$$x_i(k) = \sum_{l=0}^{L-1} \sum_{j=1}^{n} h_{ij}(l) s_j(k-l) + \omega_i(k) \quad (1)$$

where $i = 1, ..., m$ with m the number of observations/channels, so x_i represents one surface EMG channel i, $k = 1, ..., D_r$ with D_r the total number of samples , h_{ij} is the action potential of motor unit j in EMG channel i, s_j is the j-th source (motor unit spike train). $\omega_i(k)$ is additive noise regarded as stationary and a zero-mean Gaussian process, L is the total duration of the sMUAP, and n the total number of active motor units [11], [12].

This mixing model is a multiple-input-multiple-output (MIMO) system with m observations (EMG channels) and n sources (motor unit spike trains (MUSTs)). This convolutive mixing model can be rewritten in a matrix notation by representing it as an instantaneous mixture of an extended vector containing the sources s_j and their delayed versions [12]. The observations x_i are also extended to keep the ratio between observations and sources as high as possible. This creates the following matrix notation:

$$x(k) = Hs(k) + \omega(k) \quad (2)$$

where both the source $s(k)$ and observation $x(k)$ vectors must be extended with delayed versions of themselves and H contains all the sMUAP shapes and their delayed versions of the motor units across all channels. The resulting observation, source, and noise vectors are [12]:

$$x_i(k) = [x_i(k), ..., x_i(k-R)], i = 1, ..., m \quad (3)$$

$$s_j(k) = [s_j(k), ..., s_j(k-(L+R-1)], j = 1, ..., n. \quad (4)$$

$$\omega_i(k) = [\omega_i(k), ...\omega_i(k-R)], i = 1, ..., m. \quad (5)$$

with R the extension factor for the observations. A visual representation of this matrix mixing model can be seen in Figure 1.C.

B. iEMG decomposition

As the introduction states, traditional methods to decompose single motor unit activity involve intramuscular electromyogram (iEMG) recordings using fine-wire or needle electrodes [6]. Template matching algorithms have been proposed as a method for decomposing the iEMG signals, enabling full decomposition that provides insight into single motor unit behavior [7], [8]. This technique identifies iMUAPs by segmentation and classification of action potentials present in the recordings. In all decomposition algorithms, each motor unit must have a unique action potential (AP) for successful decomposition, as distinguishing between two motor units with identical APs is impossible [29]. iEMG ensures this uniqueness due to its high bandwidth, since its location close to the source. This minimizes the low-pass filtering effect caused by the tissue separating the fibers (sources) from the recording site, which is known as the 'volume conductor' [12], [30], which makes it a highly selective method. However, the main limitation of iEMG decomposition is its inability to resolve superimposed iMUAPs often resulting in incomplete action potential trains and the low amount of motor units that can be identified/detected [6]. Thereby, it is an invasive and fragile method that can cause discomfort for some subjects and during certain movements.

C. HD-EMG

Recording from the surface of the muscle can help overcome the limitations of iEMG recordings. In surface EMG (sEMG), the recording site is farther from the source than in iEMG, leading to two major differences. First, sEMG captures signals from a larger number of motor units due to the spatial distribution of signals caused by the volume conductor [12]. This reduces selectivity, as multiple motor units contribute to recordings at a specific location. Second, the volume conductor acts as a low-pass filter, decreasing the signal bandwidth which removes information from individual sMUAPs [12]. This makes sMUAPs from different motor units appear similar in surface recordings [31]. As mentioned earlier (section II-B), successful decomposition requires each motor unit to have a unique action potential (AP) in the recording [29], which poses a significant challenge for sEMG recordings. To improve discrimination of action potentials of different motor units, high-density EMG (HD-EMG) systems have been proposed [32]. These systems use multiple electrodes distributed across the muscle surface to enhance spatial resolution, capturing variations in sMUAPs across different locations. The multi-channel EMG model of section II-A represents the generation of recordings with such HD-EMG systems. With the use of convolutive filters, this model can be inverted to identify the sources from the observations.

D. Blind source seperation

To find the sources based on the observations, the sources can be extracted by estimating convolutive filters with blind source separation (BSS) techniques. Independent component analysis (ICA) is a BSS technique that does not require knowledge about the sources $s(k)$ or mixing matrix H, but two requirements must be satisfied;

- The first requirement is that there are no more sources than channels/observations [12], [33]. This requirement is in principle not satisfied as, on average, there are more identifiable motor units than electrodes on HD-EMG grids. However, if it is accepted that only a subpart of motor units - those contributing the majority of the energy to the observations - can be identified, the requirement is satisfied. In this way, the motor units that can not be identified contribute to the noise of the model [12]
- The second requirement is that all sources should be independent from each other [12].

Recent algorithms combine aspects of both FastICA [34] and convolutive kernel compensation (CKC) algorithms [11], [35] to find the underlying sources.

The first step is to extend and whiten the observations also known as 'convolutive sphering' [36]. To satisfy the first requirement for ICA in the presented extension model (eq. 2), the product between the extension factor R and the number of available channels m should be approximately equal or greater than the number of identifiable sources n multiplied by the duration of the sMUAPs (L) in samples resulting in the following condition [12].:

$$mR \geq n(L) \quad \text{or} \quad R \geq \frac{nL}{m}. \tag{6}$$

Therefore the extension factor R must satisfy equation 6. Whitening is performed to decorrelate the observations and ensure they have unit variance to satisfy the second requirement for ICA [33]. After, a fixed-point algorithm estimates the sources by maximizing their sparseness through a contrast function [18], [36]. The sources are estimated by applying a transformation matrix that maps the observations to their corresponding sources [12]. This transformation is expressed as:

$$s_j(k) = w_j z(k) \tag{7}$$

with w_j the filter that transforms the observations into the spike train s_j of the j-th motor unit. The filter w_j is refined by enhancing the non-Gaussianity of the resulting source s_j by using a cost function $g(s)$ [12]. Since each source (motor unit spike train) is assumed to be independent, the seperation vector creates a linear combination of the whitened observations z. This linear combination isolates one single source s_j, which supresses the contribution of other sources and thereby maximizes the non-Gaussianity of the extracted source [12]. The cost functions $g(s)$ are all measures for non-Gaussianity, e.g. $g(s) = \log(\cosh(\text{s}))$ or $g(s) = \exp(\frac{s^2}{2})$ [33]. This is done with the following equations:

$$w_{\text{new}}(n) = \mathbb{E}\left[g\left(w_{\text{old}}^T z\right) z\right] - A w_{\text{old}}, \tag{8}$$

with

$$A = \mathbb{E}\left[g'\left(w_{\text{old}}^T z\right)\right], \tag{9}$$

where g is a cost function that maximizes the sparsity of the resulting source w_j. An additional Gram-Schmidt orthogonalization step is used to maximize the number of estimated unique sources [33]. A second refinement step was proposed as FastICA may converge to unreliable sources [12], [37]. This step uses the CKC algorithm to refine the found separation filters through an iterative scheme. Instead of estimating the separation vector directly, CKC refines the cross-correlation vector $c_{s_j,z}$ between the j-th source s_j and the whitened extended observations z, with the following equation:

$$s_j = c_{s_j z}^T C_{zz}^{-1} z, \tag{10}$$

where $w_j = c_{s_j z}^T C_{zz}^{-1}$. The separation vector $c_{s_j z}$ is the correlation vector between the source s_j and the whitened extended signals z. C_{zz} is the covariance matrix of the whitened extended signals z and calculated as $C_{zz} = E[z(k)z^T(k)]$ İn the case of whitened observations, $C_{zz} = I$ for the white matrix z, so $w_j = c_{s_j,z}$. The initial estimate of $c_{s_j,z}$ is made with

$$c_{s_j,z} = \frac{1}{J}\sum_{i-1}^{I} z(t_i), \tag{11}$$

where J is the number of peaks the Fast-ICA algorithm found and t_i the indices at which spikes occurred. Every iteration, a peak detection algorithm gets applied to the squared of the source (MUST) and K-means classification divides the identified peaks into either noise or spikes [18], [38].The algorithm iteratively updates the separation vectors by minimizing the covariance of the spike train (CoV_{ISI}) intervals through gradient-based optimization methods [12], [18].

After, Negro et al. proposed to minimize the CoV_{ISI} given by

$$CoV_{ISI} = \frac{\text{std}(ISI)}{\text{mean}(ISI)}. \tag{12}$$

This favors regular spike trains, which is why it can used to exclude multiple mixed motor unit spike trains [18]. A summary of the pseudo-code of this algorithm is given in table I [18].

E. Evaluation of decomposition accuracy

To ensure accurate decomposition, several different metrics have been proposed. A classic approach to valuating accuracy is the 'two source' validation comparing iEMG and HD-EMG decomposition against each other. This provides a conservative estimate, as it is unlikely that both methods will make the same mistake. [12]. For this type of comparison the rate of agreement (RoA) between iEMG and HD-EMG decomposition is used and computed as:

$$RoA = \frac{C}{C + I + O}, \tag{13}$$

where C represents the number of discharges identified by both iEMG and HD-EMG decomposition within a tolerance window of ± 0.5 ms, I is the number of spikes detected solely by iEMG, and O is the number of spikes identified solely by HD-EMG decomposition.

A second metric introduced by Holobar et al. is the pulse-to-noise ratio (PNR), which showed a high correlation with decomposition accuracy, [39]. It is computed directly from the estimated spike trains, allowing accuracy estimation without the need for external validation.

Negro et al. introduced the silhouette value (SIL), a metric similar to the PNR but normalized and directly related to the RoA in isometric conditions [18]. The SIL is calculated as $SIL = \frac{b-a}{\max(b,a)}$, where b is the distance between the spike points and the noise cluster center, and a is the distance between spike points and the spikes cluster center.

F. Online Decomposition

The CKC method can also be applied directly to non-whitened extended observations x. In this case, the algorithm can be presented in the following way:

$$s_j = c_{s_j x}^T C_{xx}^{-1} x, \tag{14}$$

TABLE I
PSEUDO-CODE FOR OFFLINE DECOMPOSITION [40]

Algorithm: Offline decomposition of MU activity
1. Convolutive sphering: extend and whiten observations x
2. Initialize vector $w_j(0)$ and $w_j(-1)$
3. Fixed-point algorithm
while $\lvert w_j(n)^T(n)w_j(n-1) - 1\rvert < tol\rvert$
3a. Fixed point algorithm: $w_j(n) = \mathbb{E}\left[g\left(w_j^T(n-1)z\right)z\right] - Aw_j(n-1)$ with $A = \mathbb{E}\left[g'\left(w_j^T(n-1)z\right)\right]$
3b. Orthogonalization $w_j(n) = w_j(n) - BB^T w_j(n)$
3c. Normalization $w_j(n) = \frac{w_j(n)}{\lvert\lvert w_j(n)\rvert\rvert}$
3d. Set n = n+1
4. Initialize CoV_{n-1} and CoV_n
5. CKC algorithm
while $CoV_n < CoV_{n-1}$
5a. Estimate the j-th source with eq. 10 . $s_j = c_{s_j,z}C_{zz}^{-1}z$
5b. Apply peak detection and classify peaks with K-means classification
5c. Set $CoV_{n-1} < CoV_{n-1}$
5d. Recalculate $w_j(n)$ with newfound spikes with eq. 11.
6. Quality check
if SIL $>$0.9
6a. Accept the source estimate s_j

with c_{s_jx} the cross correlation vector (i.e. dewhitened vector w_j) and C_{xx} the covariance matrix of the extended observations x [12]. This approach is frequently utilized in real-time or online applications due to the need for rapid computation [26]. The idea behind online decomposition is to reuse decomposition parameters obtained during an offline session and applying them to live data collection [41]. These decomposition parameters include the separation filter bank w, spike and noise centroids, and spike train normalization factors. For every batch of data in online decomposition, a source estimate with eq. 14 is made. After normalization and peak detection, the peaks are classified as either spike or noise based on their Euclidean distance to either of the centroids.

G. Applications of Motor Unit Spike Trains

The individual motor unit spike trains resulting from either iEMG or HD-EMG decomposition provide valuable insights into force generation mechanisms of muscles during isometric contractions [13]. Due to the low-pass filtering effect of muscle fiber twitches and the non-linearity of motor units, the low-frequency component of common synaptic input to all motor units regulates the muscle force production [13], [14]. These working mechanisms were captured using cumulative spike trains (CSTs), which is a sum of individual motor unit spike trains resulting from decomposition [14]. Additionally, analysis of individual MU spike trains has revealed changes in MU characteristics due to fatigue [42], pain [43], and exercise [44].

The CKC algorithm proposed by Holobar et al. [3] has been shown to give reliable results even with highly synchronized sources. This enables this technique to be used in impaired individuals such as tremor patients, who suffer from higher motor-unit synchronization than healthy subjects [3], [12]. The CKC algorithm already has been shown to be effective for analyzing the mechanisms behind essential tremor. Analysis of CSTs showed a common input at the tremor frequency across motor unit pools [15].

Also, motor unit spike trains have already been used to validate rehabilitation techniques in vivo. Research on incomplete spinal cord injury (SCI) patients has shown a decrease in coherence between motor unit pools after trans-spinal electrical stimulation, which may indicate a reduction in the strength of common synaptic input to these pools [4].

Further insight into the behavior of individual motor units in movement can also be used in Human-Machine Interfacing (HMI). Current methods for the control of wearable robotics are focused on the use of EMG envelopes that also suffer from changes in MUAP shape and changing measurement conditions [17]. New methods have been proposed that focus on the use of motor unit spike trains to extract neural activity from HD-EMG recordings and have shown to be better predictors for muscle force and joint torque than conventional EMG envelopes [16], [17], [45].

H. Dynamic conditions and adaptive algorithms

Tracking activation patterns of motor units online and in real time remains challenging. For the decomposition algorithm to work in real-time, it is essential that the underlying sMUAP shapes of a motor unit stays consistent, i.e., stationary, throughout a measurement. While it is generally true that sMUAP shapes can remain relatively consistent during isometric contractions, this consistency has limitations as even in isometric conditions, sMUAP shapes are influenced by fatigue and changes in firing patterns over time [22], [46]. On top of that, to unlock the potential of BSS techniques for rehabilitation strategies or prosthetic control (described in section II-G), these findings need to be generalized to dynamic conditions. In dynamic movements such as walking or hand motions, sMUAP shapes continuously change due to factors like fatigue [22], the relative position of the electrode with respect to the innervation zone (IZ) and tendon [20], and fluctuations in volume conduction between the source and the electrodes. Studies have shown that sMUAP shapes vary with changes in joint angles [21], primarily because the electrode's position relative to the muscle's IZ and tendon shifts, changing the signal characteristics and sMUAP shapes [19], [20]. This effect is significant during dynamic movements, where muscle shortening causes uneven shifts in tendon and IZ positions relative to the recording sites, leading to changes in sMUAP shapes [20]. To adapt to changing measurement conditions, recent studies have proposed adaptive algorithms that update the separation filters and covariance matrices in real-time based on new data. Chen et al. have shown superior performance of an adaptive approach in both isometric and slow dynamic contraction in both simulated as experimental data [26]. Yeung et al. showed differences in sMUAP and iMUAP shapes and superior performance of their adaptive

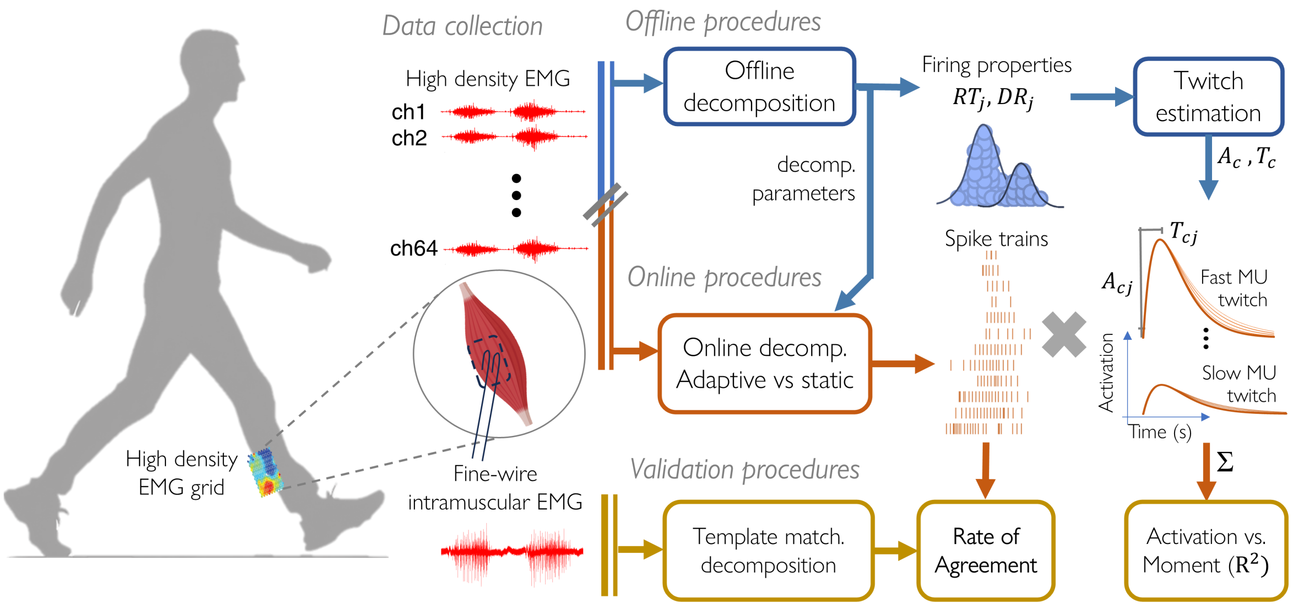

Fig. 2. Study overview. HD-EMG and iEMG signals from the m. soleus are recorded during walking and sub-maximal push-off trials. HD-EMG data is split (50/50) into training and test sets. Offline decomposition extracts MU firing properties and online decomposition parameters from training data, which are then applied to test data in a pseudo-online approach. Static and adaptive algorithms are compared to benchmark iEMG spike trains (template matching). MU activation patterns and the EMG envelope are evaluated against ankle joint moments derived from inverse dynamics. RT, DR, A_c, and T_c represent recruitment threshold, discharge rate, twitch amplitude, and contraction time, respectively.

algorithms across varying joint angles and force levels with validation through iEMG benchmarks [28]. Mendez et al. proposed an adaptive algorithm with optimized parameters that is generalizable across multiple subjects [27]. However, all of these studies apply the adaptive algorithm to slow dynamic hand movements, which limits their generalisability to walking and their application in fast dynamic movements. To date, only one study has tried HD-EMG decomposition during walking, in which only an offline and static approach was used for decomposition [47]. In summary, adaptive algorithms have shown promise in static and slow dynamic conditions. However, further research is needed to adapt these methods for real-time motor unit tracking during dynamic movements like walking.

III. Methods

Overview of the framework

This thesis proposes a framework that comprises three main components (Fig. 2). The first component is an offline procedure that uses a training dataset comprising low-force isometric and walking trials to determine decomposition parameters and optimal twitch characteristics (Section III-B.1). The second component uses the offline-acquired decomposition parameters and implements them in an online-ready framework using static and adaptive algorithms. Both approaches use the derived twitch characteristics to produce MU-specific activation dynamics (Section III-C). The last component validates the results by comparing HD-EMG decoded firing patterns with their iEMG benchmark and compares the total activation dynamics to their respective ankle moments (Section III-D). An overview of the processing pipeline can be found in appendix -A.

A. Data Collection

In total, four healthy subjects were participants were measured for this thesis. However, in only two subjects common motor units were found. Therefore, these will only be included in the results. The measurement procedure for every subject is described below. All procedures were approved by the ethical committee CMO region Arnhem-Nijmegen (protocol ID: NL73230.091.20).

1) Participant preparation: The skin of the soleus muscle was prepped by shaving and abbreviating the site at which the HD-EMG grid was going to be placed. To maximize the likelihood of detecting common motor units between iEMG and HD-EMG recordings, a bipolar fine-wire electrode was inserted superficially into the medial soleus (1 cm under the skin's surface) to record the activation of superficial muscle fibers. The iEMG recordings were made using a TMSi REFA amplifier (TMS International B.V., Oldenzaal, The Netherlands) with a sampling frequency of 17295 Hz. An 8x8 HD-EMG electrode grid (4.5mm of inter-electrode distance) was placed over the area where the tip of the fine wire electrode was located. The HD-EMG recordings were made using the TMSi SAGA 64-channel EMG amplifier with a sampling rate of 4000 Hz. After the feet, lower legs, upper legs, pelvis and torso were covered with markers to track their motion in time.

2) Motion analysis: The motion capture data and ground reaction forces (GRFs) were simultaneously recorded using a motion tracking system (Qualisys, Goteborg, Sweden, 100 Hz) and a force plate threadmill (Bertec Co., Columbus, OH, USA, 2000 Hz). OpenSim was used to retrieve ankle angles and moments from marker trajectories and GRFs via inverse kinematics and inverse dynamics [48].

3) Experiment protocol: First, a static trial was recorded for calibration and scaling of the OpenSim model. After, the participant was instructed to do 3 walking trials of 1 minute at different speeds. In the first trial, the participants were instructed to walk at their preferred 'normal' speed ($\sim$ 0.6 m/s). After, the participants were instructed to walk at a slow speed ($\leq$0.4 m/s). The second participant was also instructed to walk at a fast speed (1.0 m/s). During the walking measurements, a metronome was used to maintain a consistent cadence to ensure a steady walking pattern. After, sustained push-off trials were done at sub-maximal force levels ($\sim$30% MVC) intended for extracting low-threshold MUs.

4) Signal Processing: To eliminate noise, all of the data of HD-EMG and iEMG was filtered. A signal quality check was done for all HD-EMG channels and poor-quality channels (low signal-to-noise) were excluded using a mask. After, a 10-500 Hz fourth-order Butterworth bandpass filter was applied. To ensure distinctive iMUAPs, the iEMG signals were first re-referenced (average re-referencing) and then filtered using a first-order high-pass Butterworth filter at 1000 Hz [8]. A signal quality check was performed to see if identifiable MUAPs were present and to assess whether excessive superimposed MUAPs could hinder decomposition. If a trial did not meet these criteria, it was excluded. Further details on iEMG decomposition can be found in III-D.1 [8]. Each walking trial was split 50/50 into training and test datasets. The training data was used to estimate decomposition parameters including MU filters, centroids, and EMG masks through an offline procedure (described in Section III-B.1). In this offline approach, decomposition parameters were derived from a low-force push-off trial (30 % MVC) and the walking train data. These offline-initialized decomposition parameters were then applied to the test data of the same trial to assess the pseudo-online decomposition, comparing the performance of the static and adaptive algorithms against iEMG benchmarks.

B. Offline Procedures

1) Offline parameter estimation: The HD-EMG recordings were extended with an extension factor of 16 and the extended signals were whitened using singular value decomposition. The described fixed-point algorithm (section II-D) [18] was then applied to increase the sparsity of each source (s_j) with the update rules of equation 8 and 9. For the first iteration, the initial separation vector ($w_j(0)$) was defined as the point with the maximum squared sum of the whitened extended signals (z) across all time points. This represents the instance with the highest signal activity, which may correspond to one or more MU discharges [11]. The $g(s) = \log(\cosh(\mathrm{s}))$ contrast function was used to measure the level of sparsity of each source and the sparsity was iteratively maximized until convergence was reached (tolerance: 10^{-4}). This process is described in Step 3 of table I.

As described in Section II-D, the fixed-point algorithm may converge to unreliable sources [37]. To address this, a refinement algorithm was employed to improve the estimation of the MU spike trains. The initial separation vector (w_j) for this refinement step was calculated using Eq. 11. In this equation, the vector (w_j) is initialized as the mean of the whitened signals (z) at the time indices (t_i) corresponding to detected spikes, with J representing the number of peaks identified by the Fast-ICA algorithm.

Following this initialization, MU spike trains were estimated by squaring the source signals obtained from Eq.10, followed by identifying peaks with a minimum separation of 20 ms (equivalent to 50 Hz). These identified peaks were then classified as either spikes or noise using K-means clustering [18], [38], [49]. The source refinement process was iteratively performed until the maximum silhouette value (SIL) was achieved [16]. The SIL value was chosen because maximizing CoVISI would lead to regular discharge patterns. However, in our recorded data, a high discharge variability is expected due to the rapid rate of force development in the m. soleus during push-off. 75 iterations of this offline decomposition were run on each training dataset.
To decode a wide range of MU types, this thesis adopted a previous developed methodology to detect low threshold MUs. Motor units were decomposed on a isometric low force-push off trial [16] by minimizing the CoVISI of the spike trains [18]. MUs were accepted if $CoV_{ISI} \leq 0.5$ and SIL ≥ 0.87. After, the filters were optimized through the refinement algorithm on the walking data, where the SIL was maximized. The resulting spike trains were compared to those found in walking trails and duplicates were removed (common discharges $> 30\%$) and the spike train with the highest SIL was kept. The final step involved visually inspecting the motor unit estimates, and any noisy estimates were removed from the results.

This offline initialization decomposition parameters yielded a set of MU filters, classification centroids, covariance matrix, extension factor, EMG mask (with good-quality channels), and normalization factors for each speed.

2) MU twitch properties estimation: To model the twitch responses of each MU, the second-order system approach from Fuglevand et al. [50] was used. The model is represented as

$$a_0(t) = \frac{A_c}{T_c}\ t \exp\frac{1-t}{T_c} * u(t) \tag{15}$$

where A_c is the peak amplitude, T_c is the contraction time and $u(t)$ is the MU spike train. The peak amplitude (A_c) and contraction time (T_c) were initially estimated based on previous work that classified various MU types and their twitch properties [45], [51]. In this way, initial estimates of the twitch properties and activation dynamics of every MU can be made. However, since this methodology was only tested on isometric data, it might not estimate the twitch responses of the MUs in dynamic movements accurately. Therefore, an extra step was employed which maximized the correlation between the modeled MU-specific activation and the corresponding ankle moment. The twitch responses were iteratively optimized by reducing the contraction times (T_c) and adjusting the sparseness of the peak amplitudes so that

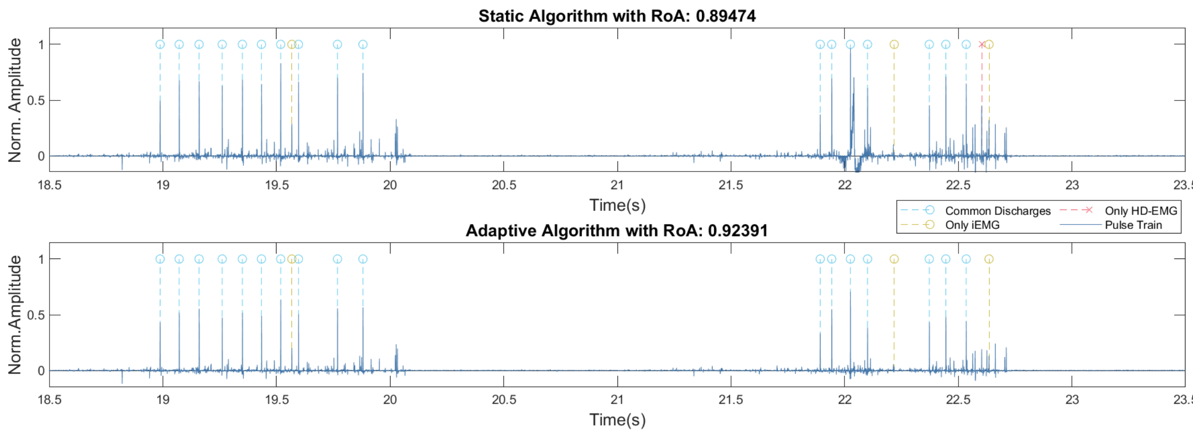

Fig. 3. Validation of HD-EMG decoded spike trains and iEMG benchmarks for both static and adaptive decomposition (representative example, subject 2, walking speed: 0.4 m/s)

the delay between ankle moment and activation decreased and the correlation improved. In this way, the responsiveness of the twitch model was enhanced while maintaining a strong correlation with the ankle moment [16].

C. Online procedures

In the online procedure, decomposition parameters initialized offline were applied to the test data to estimate spike trains. Two decomposition approaches static and adaptive were used, and their performance was compared against iEMG benchmarks. To simulate an online setting, the test data was divided into batches of varying sizes and processed using the online decomposition algorithm. Each batch overlapped with the previous one by 20 ms (80 samples at (fs = 4000 Hz) to ensure the required 20 ms peak separation.

1) Adaptive decomposition: Due to the variation of sMUAP shapes both between and within measurements, this thesis introduces an adaptive algorithm that updates the decomposition parameters in real-time to adjust to these changes. While several adaptive methods have been proposed [26]–[28], none have been applied to walking trials or highly dynamic movements. This thesis' approach combines elements from the algorithms of Chen et al. and Yeung et al., integrating their strengths to ensure robust performance. The adaptive algorithm works with the non-whitened version of the CKC (eq. 14) and introduces changes to the covariance matrix and separation vectors described in section II-F.

The first step in each batch is to update the covariance matrix with [28] (16):

$$C^*_{xx} = (1-\lambda)\cdot C_{xx} + \lambda \cdot C_{\Delta x \Delta x}, \tag{16}$$

in which λ is the learning rate and $\Delta\bar{x}$ the extended EMG signals in the new batch. Next, every motor unit spike train is iteratively estimated with Eq. 14 where the new covariance matrix C^*_{xx} is used. After peak detection, the peaks were classified based on their Euclidean distance to either the spike or noise centroids. If any spikes are detected, they are added to the spike set Ψ_i. Now, the filter was updated with (17), which is essentially a weighted average of the original separation filter and the contribution of the data in

TABLE II

Algorithm: Real-time adaptation of MU filters
1. Update C^*_{xx} with eq. 16 $C^*_{xx} = (1-\lambda)C_{xx} + \lambda C_{\Delta x \Delta x}$ **2. Adaptive source extraction**   **For every $j-th$ seperation filter s_j**
2a. Do source estimation with eq. 14 $s_{j,\text{win}} = c_{s_j} C_{xx} \Delta x$
3. Peak detection   4. Calculate Euclidian distance to spike and noise centroids T_{ij} **if any spikes are detected**
4a. Update c_{s_j} based on the new spikes Ψ_i $c_{s_j x} = (1-\lambda)\cdot c_{s_j,x} + \lambda \cdot \frac{1}{\text{card}(\Psi_i)} \sum_{n_k \in \Psi_i} x(n_k).$ 4b. Update the centroids T_{ij} 4c. Accept the updated covariance matrix $C_{xx} = C^*_{xx}$

the incoming batch:

$$c_{s_j x} = (1-\lambda)\cdot c_{s_j,x} + \lambda \cdot \frac{1}{\text{card}(\Psi_i)} \sum_{n_k \in \Psi_i} \bar{x}(n_k), \tag{17}$$

where the card represents the number of spikes in the set. The centroids were updated with the following weighted average calculation adopted from Chen et al. [26](18):

$$T^*_{ij} = \frac{w_1 T_{ij} + w_2 T'_{ij}}{w_1 + w_2}, \quad i = 1, 2, \tag{18}$$

where T_{ij} is the centroid of the previous iteration with (i=1) the spike and (i=2) noise the noise centroid for the j_{th} spike train, the T'_{ij} the mean of new spikes and T^*_{ij} the new weighted average which is saved for the next iteration. The weights $w1$ and $w2$ are the weighting factors for the old and new centroids respectively. Weighting factor $w1$ is set to 5 empirically and $w2$ as the number of new spikes in the current batch [26]. λ was set at 0.05 empirically. Table II shows the pseudo-code of the updating policy for the adaptive algorithm.

2) Static decomposition: To compare the performance of the adaptive approach, the offline-determined MU filters were re-used to estimate the sources using Eq. (10). In this static approach, sources were normalized with the previously identified normalization factors, and spike classification was

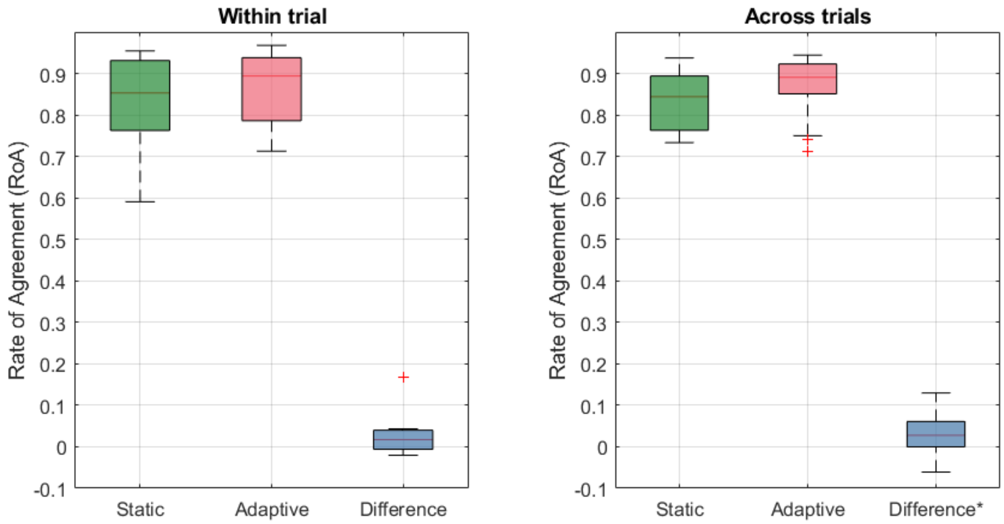

Fig. 4. A comparison of RoA between static and adaptive decomposition for all common motor units in both subjects. The left figure presents the RoA of common motor units when applying offline-initialized filters to test data at their respective speeds. The right figure illustrates the RoA of common motor units by comparing iEMG and HD-EMG decomposition, applying offline-initialized filters across test data from all speeds within a subject. To use the filters across all speeds, a common mask was used to mask the bad channels in the data. The * indicates a statistical icates a significant difference ($p<0.05$)

performed using the centroids obtained from the offline procedure.

3) MU-specific activation dynamics: To compute MU activation profiles online, the activation was discretized [52] to filter each spike train with its offline-estimated twitch model. The combined contributions of all MUs were summed to define the overall muscle activation.

D. Validation procedures

1) iEMG template matching: A benchmark decomposition was done on the iEMG recordings using EMGlab [8]. This algorithm can decompose superimposed MU waveforms by using template matching. Automatic decomposition was run on the iEMG recordings. Due to the dynamic nature of walking, the iMUAP of a MU might vary in amplitude and waveform throughout a gait cycle. Therefore, a reviewer visually inspected each spike and iMUAP to ensure accurate classification. Additionally, the spike instances between HD-EMG and iEMG were compared to confirm that no spikes detected in HD-EMG were overlooked. The resulting spike trains were downsampled to 4000 Hz to match the spike trains resulting from HD-EMG decomposition.

2) MU firing validation: To assess the accuracy of the static and adaptive algorithms, the spike trains produced by both methods were compared to the iEMG decomposition results. The spike trains from iEMG and the static/adaptive algorithms are considered to originate from the same MU only if their corresponding spike trains share more than 50% common discharges (C). The performance of both decomposition approaches was assessed using the following metrics; Rate of Agreement (RoA), as defined in eq. 13, is used to get a conservative estimate of the accuracy of both static and adaptive algorithms.

Also, the false negatives (FN) and false positives (FP) were computed as follows (19, 20):

$$FN = \frac{I}{I+C} \cdot 100\%, \tag{19}$$

$$FP = \frac{O}{O+C} \cdot 100\%, \tag{20}$$

3) Using MU filters across trials: To compare the performance of the static and adaptive algorithms across different conditions, each set of offline-initialized filters was applied to test data from other trials. This approach allows us to assess whether the adaptive algorithms can effectively compensate for significant variations in decomposition conditions, such as changes in sMUAP shapes [28]. It also assesses if the use of MU filters initialized in a different trial can be used to accurately estimate the sources in a new trial. To determine statistical significance, differences between the performance metrics in static and adaptive algorithms were evaluated using the Wilcoxon signed-rank test, with a $CI = 95\%$

4) MU-specific activation assessment: The coefficients of determination (R^2) were calculated per gait cycle as the square of the maximum normalized correlation between muscle activation estimates (from static and adaptive approaches, as well as EMG envelopes) and right ankle joint moments obtained via inverse dynamics. Statistical significant differences between static and adaptive algorithms were tested using the Wilcoxon signed-rank test with $CI = 95\%$.

5) Real-time assessment: To evaluate the real-time readiness of the adaptive approach, computational times per batch were recorded for both static and adaptive algorithms and their medians were calculated. All data processing and decomposition were performed using MATLAB R2024b, with the computations run with an Intel Core i7-9750H CPU (2.60 GHz) and 16 GB RAM.

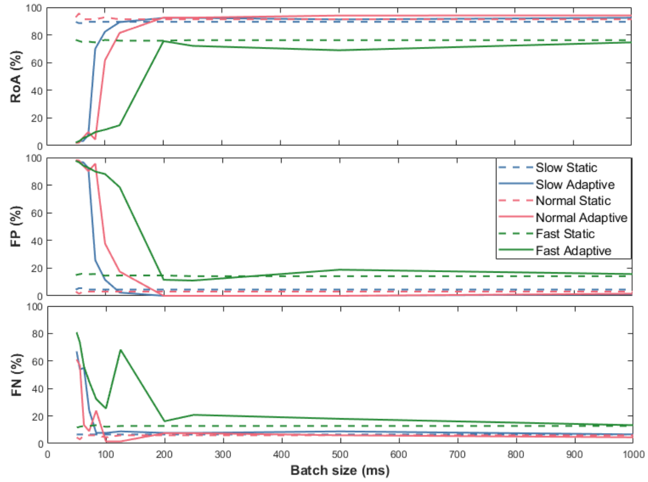

Fig. 5. Accuracy (RoA, FP, FN) across batch sizes for subject 2. the dotted line indicates the static approach and the solid line indicates the adaptive approach. Different colors indicate different walking speeds.

IV. Results

The data of both subjects suffered from synchronization issues. Therefore, the results of subject 1 only include offline initialization and validation. MU activation dynamics were only calculated for subject 2. Also, the computational times and metrics across batchsizes (fig. 5 and fig.6) are only based on the results of subject 2 as these results were synced and analyzed first.

A total of six walking trials were analyzed. Subject 1 completed two trials at a slow speed (0.3 m/s) (referred to as 0.3_1 and 0.3_2) and one at normal speed (0.6 m/s), while subject 2 performed trials at slow (0.4 m/s), normal (0.6 m/s) and fast (1.0 m/s) speeds.

During post-processing, channels 23 and 24 of HD-EMG in subject 2 were found to be too noisy by visual inspection. In Subject 1, different noisy channels across measurements were observed. As a result, a unique mask was applied to each measurement. However, for cross-use of filters, a common mask was determined, which excluded channels 1 and 58.

In table III, the results of offline-initialization of MUfilters are shown for every trial in every subject. The walking MUs indicate how many MUs were identified in the train data of the walking trial. The low-force MUs indicate how many MUs were identified in the low-force isometric trial. The Extra Refined MUs indicate how many extra MUs were identified by refining the low-force MUs on the train data of the walking trial. In subject 1, the amount of identified low-force MUs between trials differed, as different masks were used for every trial in decomposition. The mean SIL indicates the average and standard deviation of the SIL values of the found motor units. Lastly, the common MUs indicate how many common MUs were found between HD-EMG and iEMG within the trial.

Figure 3 shows a representative example are the spike trains of static and adaptive decomposition in the slow-speed measurement of subject 2 with the ground truth iEMG decomposition as reference. Figure 4 shows the distribution of RoA for all common motor units identified in both subjects, grouped into two categories. The left boxplot represents the RoA of common motor units when offline-initialized MU filters were applied to test data from the same trial. The right boxplot shows the RoA when the MU filters were used across all trials, demonstrating the performance in varying conditions.

Different batch sizes were tested with predetermined learning factors to analyze the effect on the accuracy of the adaptive algorithms. A summary of the results can be seen in figure 5, where the RoA, FP, and FN over different batchsizes are plotted. The adaptive algorithm outperforms the static algorithm in the slow and normal speeds for batchsizes greater than 200 ms in terms of RoA and false positives. For slow to normal speeds ($\leq$ 0.6 m/s), RoAs $>$ 89% were found for both static and adaptive algorithms. To assess the real-time applicability of the adaptive algorithm the computational times were Fig. 6 shows the median computational times for both static and adaptive algorithms across batch sizes. The median computation times of adaptive algorithms exceed 250 ms for all batch sizes.

Figure 7 shows the cross-use of all offline-initialized filter sets across the test data of all the trials with both the static and adaptive algorithms. It shows a significant improvement of RoA by the adaptive algorithm compared with the static algorithm ($p < 0.05$). No significant differences were found between FP and FN between adaptive and static algorithms. In the appendix, these figures can be found for subject 1. Figure 12 and figure 13 summarize the cross-use of filters for subject 1. An extensive review of the results of subject 1 is given in the appendix -B.

Figure 8 illustrates a comparison between the MU activation estimates and the joint ankle moment, along with the R^2 values for the test trial (1.0 m/s speed). The R^2 values of the adaptive and static algorithms were both higher than those of the EMG envelope ($P < 0.001$).

V. Discussion

This thesis aimed to extend the methodology to address variations in MUAP shapes during locomotion by proposing an adaptive algorithm and validating its accuracy using intramuscular EMG (iEMG) as the benchmark for decomposition. The results (see figure 4) show that the adaptive decomposition is static decomposition both within and across trials. This approach holds significant potential for real-world applications, paving the way for improved motor unit decomposition in everyday movement scenarios.

A. Adaptive Algorithm implementation

1) Rationale: This thesis proposes an adaptive algorithm that updates the covariance matrix (C_{xx}) and the separation vector ($c_{s_j,x}$) in real time by incorporating new incoming data. This enables the algorithm to adapt to changes in MUAP shapes both within and across measurements. Building on prior work that has demonstrated better performance of adaptive approaches over static ones,

TABLE III
OFFLINE INITIALIZATION OF MU FILTERS

Subject	Speed (m/s)	Walking MUs	Low-Force MUs	Extra Refined MUs	Mean SIL (SD)	Common MUs
Subject 2	Slow (0.4 m/s)	11	12	2	0.920 (0.0294)	1
	Normal (0.6 m/s)	14	12	2	0.920 (0.0394)	1
	Fast (1.0 m/s)	11	12	6	0.920 (0.0344	1
Subject 1	Slow_1 (0.3 m/s)	10	12	1	0.910 (0.0362)	2
	Slow_2 (0.3 m/s)	6	12	6	0.891 (0.0392)	1
	Normal (0.6 m/s)	8	12	0	0.93 (0.0234)	1

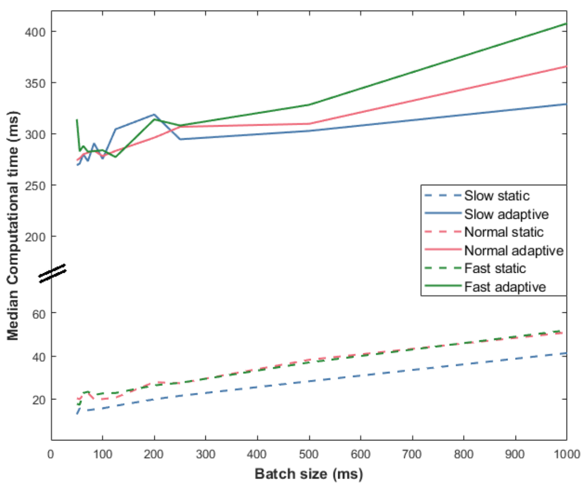

Fig. 6. Computational time (ms) across batch sizes for subject 2. The dotted line indicates the static approach and the solid line indicates the adaptive approach. Different colors indicate different walking speeds.

we initially considered Chen et al.'s summation-based update method [26] for both the covariance matrix and the separation vector. However, when applied to walking data, this approach encountered stability issues, likely due to covariance and filter inflation resulting from noise contamination in small data batches with minimal muscle activation.

In contrast, Yeung et al. introduced a weighted averaging strategy [28] that balances the influence of new data with prior information, which showed to be less susceptible to numerical instabilities. Consequently, our algorithm adopts this weighted averaging approach to ensure robust and reliable updates under dynamic conditions. For peak classification, preliminary analysis showed that the weighted average from Chen et al. [26]performed better than the z-score buffer approach proposed by Yeung et al. [28]. By combining Yeung's weighted updating mechanism with Chens peak classification method, the proposed adaptive algorithm showed enhanced stability and accuracy in dynamic conditions, making it a robust solution for real-time applications.

2) Stability analysis : Figure 5 shows that for small batch sizes (< 100 ms) the current combination of $\lambda = 0.05$ and $w_1 = 5$ results in really low RoA. The explanation for this lies in the stability of spike train estimation. For small batch sizes, noise gets added to the cross-correlation vector and covariance matrix, which results in noisy estimates. A visual example of such a noisy estimate of spike trains be found in appendix -C. For bigger batch sizes (≥ 100 ms), the chosen parameters were able to estimate the spike trains reliably and accurately. Further investigation into the optimal parameter values for smaller batchsizes is preferred, as this would allow the adaptive algorithm to cover intra-step changes in the sMUAP, i.e MUAP shape changing within a gait cycle. Chen et al. [26] show good performance of 200 ms batches across multiple rates of change for sMUAP shapes, which might be a good starting point.

B. Static versus adaptive algorithms in changing MUAP shapes

The left plot of figure 4 shows the results of applying the offline-initialized filters to their corresponding test data. Although not statistically significant, the difference between static and adaptive decomposition is mainly positive, which indicates a superior performance of the adaptive approach compared to the static approach. For subject 2, the static algorithm showed RoAs $\leq$ 89% in both slow ($\leq$ 0.4 m/s) and normal (0.6 m/s) walking speeds (see figure 7). For subject 1, the static algorithm also showed high RoAs $\leq 85\%$ in both slow trials ($\leq$ 0.4 m/s) (see figure 11). This shows that even static decomposition performs well in slow walking movements for the m. soleus. This is supported by other studies that already applied traditional BSS methods to slow dynamic movements [53]. Yokoyama et al. [54] reported high RoA and SIL for static decomposition in dynamic ankle dorsiflexion movements with a range of motion (ROM) of up to 30° in the m. tibialis anterior (TA) and later used it to characterize MU firing patterns during slow-speed walking trials [47]. They argued that static decomposition remains accurate in slow walking trials, as the ankle joint's ROM stays within 25° [55]. This thesis' findings support this reasoning for the m. soleus at slow walking speeds, since the RoA of static algorithms remains high at walking speeds up to 0.6 m/s.

One possible explanation for this result is the minimal fiber length variation of the m. soleus during the push-off phase [24], [25]. It is known that surface motor unit action potential (sMUAP) shapes change with varying joint angles [21], due to shifts in electrode positioning relative to the innervation zone and tendon (IZ), changes in volume

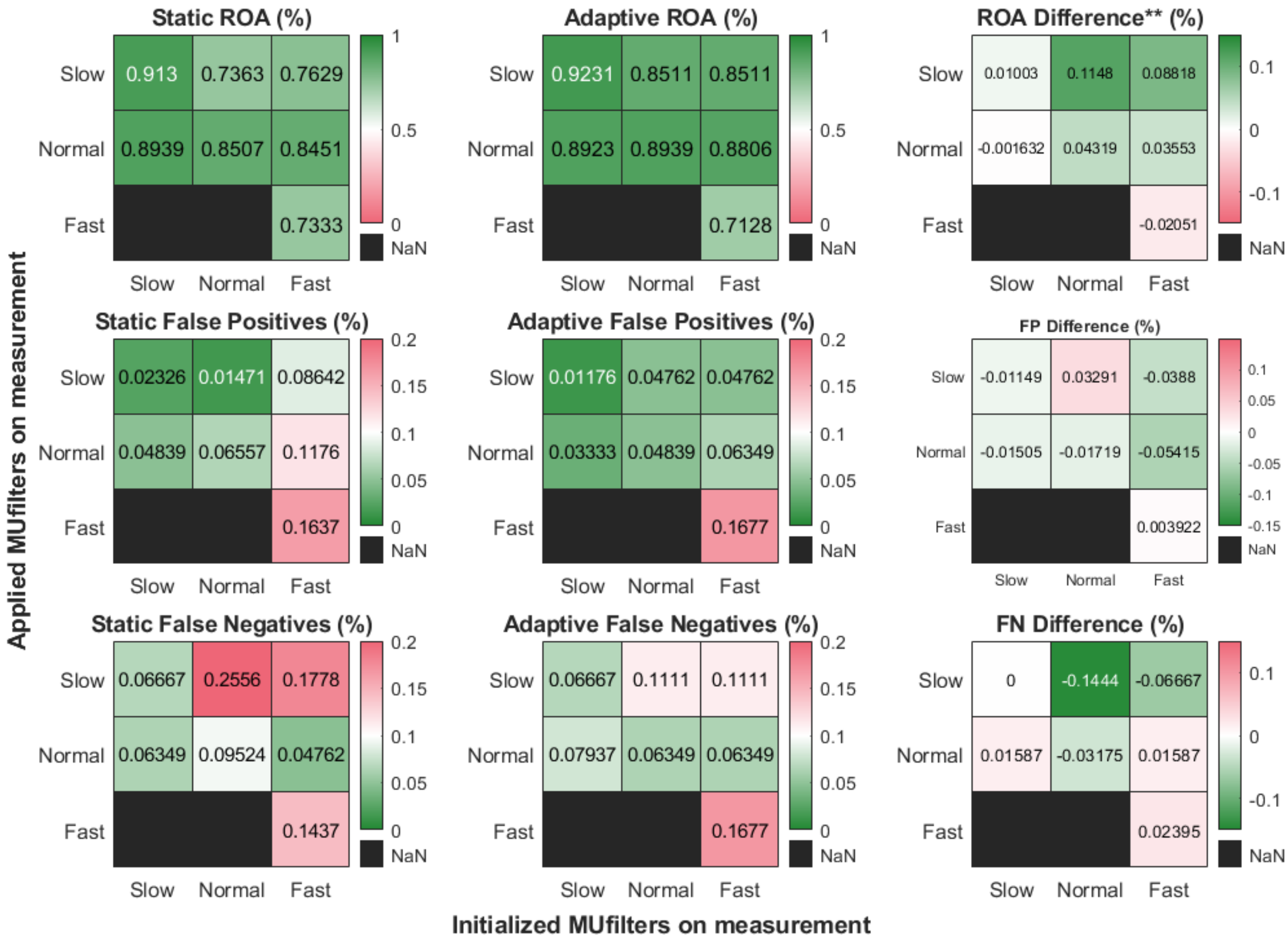

Fig. 7. Cross-comparison in Subject 2: All offline-initialized filters were tested across all speeds to assess their performance. The left and middle columns display the RoA, FP, and FN for the static and adaptive decomposition methods, respectively. The right column shows the differences in RoA, FP, and FN between the two approaches (Adaptive - Static), with green indicating better performance for the adaptive method and red indicating better performance for the static method. NaN values represent cases where no common motor units were identified between the HD-EMG and iEMG decomposition (common discharge $<$ 50%). The diagonal elements of each heatmap reflect the performance of using the offline-initialized MU filters on their corresponding test data. Asterisks (**) indicate a statistically significant difference between static and adaptive decomposition (p$<$0.05).

conduction and changes due to fatigue [22], [46]. Due to the small fiber length variation of the soleus muscle, no significant changes in the relative position of IZ and tendons with respect to the surface electrodes or changing volume conductor effects were expected, leading to only minor variations in sMUAP shapes. This may explain the strong performance of the static approach in terms of RoA, false positives (FP), and false negatives (FN) for all batch sizes (see Figure 5). Furthermore, the adaptive algorithm performed the best with a lower value of λ (0.05 rather than the 0.10 used by Yeung et al. [28]), which might further confirm that sMUAP shape variations over time are minimal.

For the fast speed in subject 2 (1.0 m/s) and the normal speed in subject 1 (0.6 m/s) , the RoA ($<$75%) is significantly lower for both static and adaptive approaches even though the training SIL-value for the filters did reach the threshold of 0.87. This would suggest that a high SIL does not always correlate with a high RoA in dynamic movements. This is in line with the findings of Yokohama et al., which showed a poor correlation between the SIL and RoA of discontinuously identified MUs [54]. However, since this study's MUs were continuously identified, this discrepancy suggests a more complex correlation between SIL and RoA in walking trials. Additionally, the algorithm responsible for removing duplicates did not always select the best-performing MU filters. This may be due to the complex relationship between SIL and RoA in dynamic movements. Alternatively, for subject 1 it could be a result of challenging decomposition conditions as it exhibited more movement artifacts, which made the decomposition process more difficult.

The validation of the framework with iEMG benchmarks demonstrated superior performance of the adaptive approach compared to the static approach for all metrics in the slow and normal speeds, particularly for windows larger than 200 ms (see figure 5 and 11). Chen et al. support these findings, as they reported a great increase in precision and sensitivity between static and adaptive algorithms in dynamic contractions in simulated data [26]. They even showed that the rate of change in sMUAP shapes did not influence the accuracy of the adaptive algorithm, which shows the robustness of the method. It should be remarked that the gains between adaptive and static algorithms are marginal as

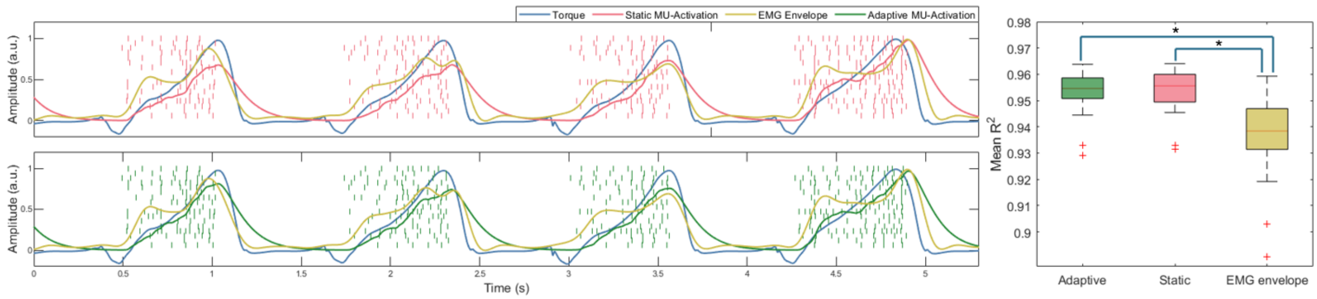

Fig. 8. Comparison between normalized activation estimates and ankle moments. Left panel: Calculated activation versus joint moment for 1.0 ms speed. Right panel: Coefficients of determination between activation estimates and ankle moments per gait cycle. * indicates significant differences (p<0.001).

the static algorithm already performed well at these speeds. At a fast speed in subject 2 (1.0 m/s), the adaptive algorithm performs even worse than the static approach, likely due to amplitude cancellation at higher force levels [23], which significantly complicates the decomposition process.

C. Static versus adaptive algorithms across conditions

Using offline-initialized filter sets across all speeds significantly improves the RoA of the adaptive algorithm compared to the static algorithm ($p < 0.05$) (see right plot of figure 4). While no significant differences in FP and FN were observed between the two algorithms, figures**??**, 12 and 13 indicate that the adaptive algorithm consistently matches or outperforms the static approach, particularly when applying filters derived from different speeds. This indicates that the adaptive approach is more effective when generalizing filters across different speeds conditions. The cross-comparison plots for both subjects suggest that applying MU filters from a higher-speed trial to a lower-speed trial performs worse than the other way around. Therefore it seems that initializing MU filters should always be done on a lower of equal speed to ensure high decomposition performance (see Figure 13).

This finding aligns with Yeung et al., who also reported superior performance of the adaptive algorithm in isometric contractions across different joint angles and force levels in forearm muscles [28]. The observed consistency across conditions highlights the robustness of the adaptive algorithm and its ability to cope with MUAP shape changes across measurements.

D. Computational time

The adaptive algorithms computation time exceeds 250 ms for all batch sizes (see Figure 6), primarily because of the high 4000 Hz sampling frequency required to capture detailed temporal information in the HD-EMG recordings. However, this computational time is too high for Human Machine Interfacing (HMI), where total computation, so recording of data and processing, should occur within the neuromechanical delay of around 200 ms [56].

The major computational bottleneck is the repeated inversion of the covariance matrix C_{xx} in each iteration, which is necessary for adaptive decomposition. The size of C_{xx} is determined by the number of channels multiplied by the extension factor R. In this study, we used 62 channels (excluding two due to poor quality) and $R = 16$, resulting in a 992×992 matrix, which is computationally expensive to invert.

For comparison, Chen et al. [26] used a sampling frequency of 2048 Hz with $R = 10$, yielding a 640×640 covariance matrix and an average inversion time of approximately 50 ms per 200 ms batch. Similarly, Yeung et al. [28] reported an average computation time of 57.1 ± 14 ms with a sampling frequency of 2048 Hz and $R = 16$. These results show that smaller covariance matrices can help to lower the total computation time considerably.

E. Translation into MU specific activation patterns

The correlations between activation patterns estimated with the static and adaptive MU spike trains and estimated joint moments were not statistically significant from each other ($p > 0.05$). One explanation might be that MU-derived activation and joint torque are not linearly related due to non-linear characteristics of musculoskeletal function [57], so linearly comparing them with correlation does not take this relation into account. However, they both outperformed the EMG envelope in terms of $R2$ value ($p < 0.05$), which might be an indication of better performance of MU-specific approaches.

One major limitation of Fuglevand's model is its inability to control the decay or relaxation phase of activation [50]. This can also be seen in our MU-specific activation patterns, where activation gradually decreases after reaching its maximum (see Figure 8). Despite this limitation, Fuglevand's model was chosen for its efficiency, as it can be discretized which makes it computationally much less expensive [52]. In contrast, models like Raikova et al. require more processing power, making them less suitable for real-time use [51].

Integrating the proposed framework with personalized neuro-musculoskeletal (NMS) models can help to further advance the [45], [48], [58]. A previous study has already linked MU-specific activation with their contractile and twitch properties to estimate ankle joint torques in isometric contractions by measuring both m. soleus and m. tibialis anterior [45]. This study found greater generalization of the MU-specific approach across conditions compared to EMG-driven models. Furthermore, this MU-specific can provide deeper insights into the neural mechanisms underlying force generation. This thesis's findings extend this methodology by directly validating the decomposition results at a MU level in dynamic contractions, a step that paves the way toward real-time control applications, such as wearable prosthetics using human-machine interfaces (HMIs). Recent advancements support this as they proposed a real-time framework that uses personalized NMS models for control of wearable robotics [59].

F. Limitations and recommendations

The thesis's primary limitation is its small sample size. Although in total four subjects were measured, only the data of two subjects could be used due to synchronization issues between measurements in two subjects and the inability to identify common motor units between HD-EMG and iEMG despite multiple attempts in the other subjects. Therefore, future research should include more participants to assess the generalizability of the method across subjects. Additionally, increasing the number of common motor units between HD-EMG and iEMG decompositions by using multiple fine-wire electrodes under the HD-EMG grid could improve the reliability of estimates, as demonstrated by Yeung et al [28].

As we used the m. soleus, it is important to test our method on other, more 'dynamic' muscles during walking. The TA, for example, shows larger relative fiber length variations in its activated state [25], which probably shows more pronounced changes in MUAP shapes throughout a gait cycle. As discussed earlier, Yokoyama et al. demonstrated that even with static decomposition both high RoA and SIL could be achieved in the tibialis anterior during dynamic ankle dorsiflexion ROM up to 30° [54]. They used these results to characterize MU firing patterns in slow walking trials [47]. However, while their work confirms that static decomposition is feasible across varying joint angles, it lacked validation at the MU level with iEMG benchmarks in walking like this thesis did. Given the high force and rapid force buildup in the TA during walking, which likely increases MUAP non-stationarity, applying the adaptive algorithm could improve accuracy over static decomposition. To investigate such sMUAP shapes changes within a gait cycle, the MUAPs could be averaged according to their specific phase within the gait cycle to analyze whether temporal variations in MUAP shape across gait are present. However, to obtain reliable MUAP estimates through spike train averaging usually 30-100 spiks are averaged [60]. This requires long measurements which are susceptible to temporal changes in sMUAP shape due to fatigue or long term changes in firing patterns [22], [46], which can interfere with the accurate estimation of the MUAP shapes.

Additionally, investigating the TA might provide valuable insight into how the parameter λ affects the accuracy of the adaptive algorithm. Since λ essentially controls the algorithms responsiveness to new data or changing conditions, a muscle with greater fiber length variability may require a higher λ value. Previous adaptive algorithms have reported using $\lambda = 0.10$, but these studies primarily focused on forearm muscles [26] and wrist flexors [28] that experience greater normalized fiber length changes than the m. soleus [25], [61]. Therefore, muscles with greater fiber length variability, such as the TA, may require a higher λ to better account for the larger MUAP shape variations during walking.

Another advantage of measuring the TA is its role as an antagonist to the soleus, which allows for a more accurate estimation of ankle joint torque. When combined with personalized neuromusculoskeletal (NMS) models, this approach can further refine torque estimations. This has already been demonstrated in previous work as it found greater generalization of the MU-specific approach across conditions compared to EMG-driven models [45]. To extend this methodology, additional time-dependent properties of the NMS system should be included, such as potentiation effects and fatigue dynamics [46], [62], to further enhance the accuracy and applicability of these models in sustained and repeated contractions.

Furthermore, this thesis has multiple implications for rehabilitation strategies and insights into the pathological mechanisms behind neuromuscular disorders. First of all, the adaptive decomposition enables the characterization of MU firing patterns in dynamic and nonstationary conditions such as walking. With the use of CSTs, the common synaptic input in multiple motor unit pools and muscles can be estimated in dynamic movements, as adaptive decomposition improves the decomposition accuracy [13] An example of such application in pathology is tremor suppression in tremor patients. Currently, models have been proposed that rely on general sEMG analysis of tremor frequencies [63]. However, further analyzing the tremor synaptic input to motor pools via CSTs can refine FES approaches. This is particularly interesting in essential tremor, as symptoms are mainly present during movement [15], [64].

It also helps to enhance personalized rehabilitation therapies. With the use of CSTs, it can be investigated what the effect of trans-cranial/functional electrical stimulation on motor unit pools in patients that suffer from SCI [4], as mentioned earlier (Section II-G). Adapting the stimulation parameters in a real-time fashion based on the spike trains resulting from this stimulation, can help to tailor rehabilitation strategies towards personalized treatments. Adaptive decomposition can help to adapt to changing conditions after stimulation in such measurements to keep the accuracy of the estimated spike trains high.

Furthermore, it can enhance the control of wearable robotics via MU-specific modeling in dynamic conditions. MU-specific approaches towards neuro-musculoskeletal modeling have already shown superior performance in isometric conditions compared to the use of conventional EMG envelopes [16], [17], [45]. However, adaptive decompositon could enable the accurate decomposition in dynamic conditions, opening up alleys towards control of exoskeletons .

However, before this framework can be applied to real-time control systems for prostheses or wearable robotics, it must be validated across a more diverse participant pool. Although the current adaptive algorithm performs well in two healthy individuals, it has not yet been validated in populations with neurological impairments such as tremor or SCI. Such validation is crucial as impairments can alter motor unit behavior, as they exhibit persistent inward currents and abnormal muscle synergies. [65], [66]. Moreover, integrating this approach with motor unit tracking methodologies could enable longitudinal studies offering valuable insights into the remodeling effects of rehabilitation strategies over time [67]. This could also help tailor rehabilitation towards more patient-specific approaches. However, this should be interpreted with caution, as neuromuscular impairments likely pose greater decomposition challenges that must first be addressed.

VI. Conclusion

In conclusion, this thesis presents an online-capable adaptive framework for motor unit decomposition from HD-EMG during walking. The approach integrates offline parameter extraction with an online adaptive algorithm to address the challenges of MUAP variations during walking, providing a robust basis for future applications in movement analysis, rehabilitation, and real-time assistive wearable robotics in dynamic conditions.

References

[1] R. M. Enoka and J. Duchateau, "Physiology of muscle activation and force generation," Apr. 2016.

[2] E. Martinez-Valdes, F. Negro, A. Botter, P. A. Pincheira, G. L. Cerone, D. Falla, G. A. Lichtwark, and A. G. Cresswell, "Modulations in motor unit discharge are related to changes in fascicle length during isometric contractions," *Journal of Applied Physiology*, vol. 133, pp. 1136–1148, 11 2022.

[3] A. Holobar, V. Glaser, J. A. Gallego, J. L. Dideriksen, and D. Farina, "Non-invasive characterization of motor unit behaviour in pathological tremor," *Journal of Neural Engineering*, vol. 9, no. 5, 2012.

[4] A. Gogeascoechea, A. Kuck, E. van Asseldonk, F. Negro, J. R. Buitenweg, U. S. Yavuz, and M. Sartori, "Interfacing With Alpha Motor Neurons in Spinal Cord Injury Patients Receiving Trans-spinal Electrical Stimulation," *Frontiers in Neurology*, vol. 11, p. 493, 6 2020.

[5] D. Stashuk, "Emg signal decomposition: how can it be accomplished and used?," *Journal of Electromyography and Kinesiology*, vol. 11, p. 151173, June 2001.

[6] E. Martinez-Valdes, R. M. Enoka, A. Holobar, K. McGill, D. Farina, M. Besomi, F. Hug, D. Falla, R. G. Carson, E. A. Clancy, C. Disselhorst-Klug, J. H. van Dien, K. Tucker, S. Gandevia, M. Lowery, K. Sgaard, T. Besier, R. Merletti, M. C. Kiernan, J. C. Rothwell, E. Perreault, and P. W. Hodges, "Consensus for experimental design in electromyography (cede) project: Single motor unit matrix," *Journal of Electromyography and Kinesiology*, vol. 68, p. 102726, Feb. 2023.

[7] R. S. Lefever and C. J. De Luca, "A procedure for decomposing the myoelectric signal into its constituent action potentials - part i: Technique, theory, and implementation," *IEEE Transactions on Biomedical Engineering*, vol. BME-29, p. 149157, Mar. 1982.

[8] K. C. McGill, Z. C. Lateva, and H. R. Marateb, "Emglab: An interactive emg decomposition program," *Journal of Neuroscience Methods*, vol. 149, p. 121133, Dec. 2005.

[9] R. Merletti, A. Holobar, and D. Farina, "Analysis of motor units with high-density surface electromyography," *Journal of Electromyography and Kinesiology*, vol. 18, p. 879890, Dec. 2008.

[10] A. Gallina, C. Disselhorst-Klug, D. Farina, R. Merletti, M. Besomi, A. Holobar, R. M. Enoka, F. Hug, D. Falla, K. Sgaard, K. McGill, E. A. Clancy, R. G. Carson, J. H. van Dien, S. Gandevia, M. Lowery, T. Besier, M. C. Kiernan, J. C. Rothwell, K. Tucker, and P. W. Hodges, "Consensus for experimental design in electromyography (cede) project: High-density surface electromyography matrix," *Journal of Electromyography and Kinesiology*, vol. 64, p. 102656, June 2022.

[11] A. Holobar and D. Zazula, "Multichannel blind source separation using convolution Kernel compensation," *IEEE Transactions on Signal Processing*, vol. 55, pp. 4487–4496, 9 2007.

[12] D. Farina and A. Holobar, "Characterization of human motor units from surface emg decomposition," *Proceedings of the IEEE*, vol. 104, p. 353373, Feb. 2016.

[13] D. Farina and F. Negro, "Common synaptic input to motor neurons, motor unit synchronization, and force control," *Exercise and Sport Sciences Reviews*, vol. 43, p. 2333, Jan. 2015.

[14] F. Negro, U. . Yavuz, and D. Farina, "The human motor neuron pools receive a dominant slowvarying common synaptic input," *The Journal of Physiology*, vol. 594, p. 54915505, June 2016.

[15] J. A. Gallego, J. L. Dideriksen, A. Holobar, J. Ibez, J. L. Pons, E. D. Louis, E. Rocon, and D. Farina, "Influence of common synaptic input to motor neurons on the neural drive to muscle in essential tremor," *Journal of Neurophysiology*, vol. 113, p. 182191, Jan. 2015.

[16] A. Gogeascoechea, M. I. Mohamed Refai, U. S. Yavuz, and M. Sartori, "Towards Real-Time Decoding of Motor Unit Firing Events and Resulting Muscle Activation During Human Locomotion and High-Force Contractions," *Proceedings of the IEEE RAS and EMBS International Conference on Biomedical Robotics and Biomechatronics*, pp. 1434–1439, 2024.

[17] M. Sartori, U. . Yavuz, and D. Farina, "In vivo neuromechanics: Decoding causal motor neuron behavior with resulting musculoskeletal function," *Scientific Reports*, vol. 7, Oct. 2017.

[18] F. Negro, S. Muceli, A. M. Castronovo, A. Holobar, and D. Farina, "Multi-channel intramuscular and surface EMG decomposition by convolutive blind source separation," *Journal of Neural Engineering*, vol. 13, no. 2, 2016.

[19] D. Farina, R. Merletti, M. Nazzaro, and I. Caruso, "Effect of joint angle on emg variables in leg and thigh muscles," *IEEE Engineering in Medicine and Biology Magazine*, vol. 20, no. 6, p. 6271, 2001.

[20] M. Barbero, R. Merletti, and A. Rainoldi, *Generation, Propagation, and Extinction of Single-Fiber and Motor Unit Action Potentials*, p. 2138. Springer Milan, 2012.

[21] V. Glaser and A. Holobar, "Motor unit identification from high-density surface electromyograms in repeated dynamic muscle contractions," *IEEE Transactions on Neural Systems and Rehabilitation Engineering*, vol. 27, p. 6675, Jan. 2019.

[22] D. Farina, M. Gazzoni, and F. Camelia, "Low-threshold motor unit membrane properties vary with contraction intensity during sustained activation with surface EMG visual feedback," *Journal of Applied Physiology*, vol. 96, pp. 1505–1515, 4 2004.

[23] K. G. Keenan, D. Farina, R. Merletti, and R. M. Enoka, "Amplitude cancellation reduces the size of motor unit potentials averaged from the surface EMG," *Journal of Applied Physiology*, vol. 100, pp. 1928–1937, 6 2006.

[24] J. Rubenson, N. J. Pires, H. O. Loi, G. J. Pinniger, and D. G. Shannon, "On the ascent: The soleus operating length is conserved to the ascending limb of the force-length curve across gait mechanics in humans," *Journal of Experimental Biology*, vol. 215, no. 20, pp. 3539–3551, 2012.

[25] E. M. Arnold and S. L. Delp, "Fibre operating lengths of human lower limb muscles during walking," *Philosophical Transactions of the Royal Society B: Biological Sciences*, vol. 366, p. 1530, 5 2011.

[26] C. Chen, S. Ma, X. Sheng, D. Farina, and X. Zhu, "Adaptive Real-Time Identification of Motor Unit Discharges from Non-Stationary High-Density Surface Electromyographic Signals," *IEEE Transactions on Biomedical Engineering*, vol. 67, pp. 3501–3509, 12 2020.

[27] I. Mendez Guerra, D. Y. Barsakcioglu, and D. Farina, "Wearable neural interfaces: Real-time identification of motor neuron discharges in dynamic motor tasks," Feb. 2024.

[28] D. Yeung, F. Negro, and I. Vujaklija, "Adaptive HD-sEMG decomposition: Towards robust real-time decoding of neural drive," *bioRxiv*, p. 2023.09.18.558259, 9 2023.

[29] D. Farina, F. Negro, M. Gazzoni, and R. M. Enoka, "Detecting the unique representation of motor-unit action potentials in the surface electromyogram," *Journal of Neurophysiology*, vol. 100, p. 12231233, Sept. 2008.

[30] D. Farina, D. F. Stegeman, and R. Merletti, "Biophysics of the generation of emg signals," Apr. 2016.

[31] D. F. Stegeman, J. H. Blok, H. J. Hermens, and K. Roeleveld, "Surface emg models: properties and applications," *Journal of Electromyography and Kinesiology*, vol. 10, p. 313326, Oct. 2000.

[32] J. H. Blok, J. P. van Dijk, G. Drost, M. J. Zwarts, and D. F. Stegeman, "A high-density multichannel surface electromyography system for the characterization of single motor units," *Review of Scientific Instruments*, vol. 73, p. 18871897, Apr. 2002.

[33] A. Hyvärinen and E. Oja, "Independent component analysis: algorithms and applications," *Neural Networks*, vol. 13, p. 411430, June 2000.

[34] M. Chen and P. Zhou, "A novel framework based on FastICA for high density surface EMG decomposition," *IEEE Transactions on Neural Systems and Rehabilitation Engineering*, vol. 24, pp. 117–127, 1 2016.

[35] A. Holobar and D. Zazula, "Gradient Convolution Kernel Compensation Applied to Surface Electromyograms," *Independent Component Analysis and Signal Separation*, pp. 617–624, 2007.

[36] J. Thomas, Y. Deville, and S. Hosseini, "Time-domain fast fixed-point algorithms for convolutive ica," *IEEE Signal Processing Letters*, vol. 13, p. 228231, Apr. 2006.

[37] T. Wei, "On the spurious solutions of the fastica algorithm," in *2014 IEEE Workshop on Statistical Signal Processing (SSP)*, p. 161164, IEEE, June 2014.

[38] Y. Ning, X. Zhu, S. Zhu, and Y. Zhang, "Surface emg decomposition based on k-means clustering and convolution kernel compensation," *IEEE Journal of Biomedical and Health Informatics*, vol. 19, p. 471477, Mar. 2015.

[39] A. Holobar, M. A. Minetto, and D. Farina, "Accurate identification of motor unit discharge patterns from high-density surface EMG and validation with a novel signal-based performance metric," *Journal of Neural Engineering*, vol. 11, no. 1, 2014.

[40] F. Negro, U. . Yavuz, and D. Farina, "Limitations of the spike-triggered averaging for estimating motor unit twitch force: A theoretical analysis," *PLoS ONE*, vol. 9, p. e92390, Mar. 2014.

[41] D. Y. Barsakcioglu and D. Farina, "A real-time surface emg decomposition system for non-invasive human-machine interfaces," *2018 IEEE Biomedical Circuits and Systems Conference (BioCAS)*, p. 14, Oct. 2018.

[42] Y. Liu, H. Zhao, Y. Sun, L. Zhang, X. Chen, and X. Zhang, "Estimating muscle force based on a neuromuscular decoding approach adaptive to fatigue conditions," *Biomedical Signal Processing and Control*, vol. 98, p. 106769, Dec. 2024.

[43] E. Martinez-Valdes, F. Negro, M. Arvanitidis, D. Farina, and D. Falla, "Pain-induced changes in motor unit discharge depend on recruitment threshold and contraction speed," *Journal of Applied Physiology*, vol. 131, p. 12601271, Oct. 2021.

[44] A. Del Vecchio, A. Casolo, F. Negro, M. Scorcelletti, I. Bazzucchi, R. Enoka, F. Felici, and D. Farina, "The increase in muscle force after 4 weeks of strength training is mediated by adaptations in motor unit recruitment and rate coding," *The Journal of Physiology*, vol. 597, p. 18731887, Feb. 2019.

[45] A. Gogeascoechea, R. Ornelas-Kobayashi, U. S. Yavuz, and M. Sartori, "Characterization of Motor Unit Firing and Twitch Properties for Decoding Musculoskeletal Force in the Human Ankle Joint In Vivo," *IEEE Transactions on Neural Systems and Rehabilitation Engineering*, vol. 31, pp. 4040–4050, 2023.

[46] J. R. Potvin and A. J. Fuglevand, "A motor unit-based model of muscle fatigue," *PLOS Computational Biology*, vol. 13, p. e1005581, 6 2017.

[47] H. Yokoyama, N. Kaneko, A. Sasaki, A. Saito, and K. Nakazawa, "Firing behavior of single motor units of the tibialis anterior in human walking as non-invasively revealed by HDsEMG decomposition," *Journal of Neural Engineering*, vol. 19, p. 066033, 12 2022.

[48] A. Seth, J. L. Hicks, T. K. Uchida, A. Habib, C. L. Dembia, J. J. Dunne, C. F. Ong, M. S. DeMers, A. Rajagopal, M. Millard, S. R. Hamner, E. M. Arnold, J. R. Yong, S. K. Lakshmikanth, M. A. Sherman, J. P. Ku, and S. L. Delp, "Opensim: Simulating musculoskeletal dynamics and neuromuscular control to study human and animal movement," *PLOS Computational Biology*, vol. 14, p. e1006223, July 2018.

[49] J. Rossato, F. Hug, K. Tucker, L. Lacourpaille, D. Farina, S. Avrillon, and M. U. Hub, "I-Spin live: An open-source software based on blind-source separation for decoding the activity of spinal alpha motor neurons in real-time," *bioRxiv*, vol. 12, p. 2023.04.14.536933, 2023.

[50] A. J. Fuglevand, D. A. Winter, and A. E. Patla, "Models of recruitment and rate coding organization in motor-unit pools," *Journal of Neurophysiology*, vol. 70, no. 6, pp. 2470–2488, 1993.

[51] A. Gogeascoechea, R. O. Kobayashi, U. S. Yavuz, and M. Sartori, "Identification of Motor Unit Twitch Properties in the Intact Human in Vivo," *Proceedings of the Annual International Conference of the IEEE Engineering in Medicine and Biology Society, EMBS*, pp. 6310–6313, 2021.

[52] R. R. Cisi and A. F. Kohn, "Simulation system of spinal cord motor nuclei and associated nerves and muscles, in a Web-based architecture," *Journal of Computational Neuroscience*, vol. 25, pp. 520–542, 12 2008.

[53] A. S. Oliveira and F. Negro, "Neural control of matched motor units during muscle shortening and lengthening at increasing velocities," *Journal of Applied Physiology*, vol. 130, p. 17981813, June 2021.

[54] H. Yokoyama, A. Sasaki, N. Kaneko, A. Saito, and K. Nakazawa, "Robust identification of motor unit discharges from high-density surface emg in dynamic muscle contractions of the tibialis anterior," *IEEE Access*, vol. 9, p. 123901123911, 2021.

[55] B. F. Mentiplay, M. Banky, R. A. Clark, M. B. Kahn, and G. Williams, "Lower limb angular velocity during walking at various speeds," *Gait & Posture*, vol. 65, p. 190196, Sept. 2018.

[56] A. Del Vecchio, A. beda, M. Sartori, J. M. Azorn, F. Felici, and D. Farina, "Central nervous system modulates the neuromechanical delay in a broad range for the control of muscle force," *Journal of Applied Physiology*, vol. 125, p. 14041410, Nov. 2018.

[57] C. P. Cop, A. C. Schouten, B. Koopman, and M. Sartori, "Electromyography-driven model-based estimation of ankle torque and stiffness during dynamic joint rotations in perturbed and unperturbed conditions," *Journal of Biomechanics*, vol. 145, p. 111383, Dec. 2022.

[58] G. Durandau, D. Farina, and M. Sartori, "Robust Real-Time Musculoskeletal Modeling Driven by Electromyograms," *IEEE Transactions on Biomedical Engineering*, vol. 65, no. 3, pp. 556–564, 2018.

[59] M. Sartori, M. I. Refai, L. A. Gaudio, C. P. Cop, D. Simonetti, F. Damonte, M. Hambly, D. G. Lloyd, C. Pizzolato, and G. Durandau, "Ceinms-rt: an open-source framework for the continuous neuromechanical model-based control of wearable robots," Jan. 2025.

[60] A. Del Vecchio, A. Holobar, D. Falla, F. Felici, R. Enoka, and D. Farina, "Tutorial: Analysis of motor unit discharge characteristics from high-density surface emg signals," *Journal of Electromyography and Kinesiology*, vol. 53, p. 102426, Aug. 2020.

[61] R. V. Gonzalez, T. S. Buchanan, and S. L. Delp, "How muscle architecture and moment arms affect wrist flexion-extension moments," *Journal of Biomechanics*, vol. 30, p. 705712, July 1997.

[62] A. Del Vecchio, F. Negro, F. Felici, and D. Farina, "Associations between motor unit action potential parameters and surface EMG features," *Journal of Applied Physiology*, vol. 123, pp. 835–843, 10 2017.

[63] E. Rocon, J. A. Gallego, L. Barrios, A. R. Victoria, J. Ibanez, D. Farina, F. Negro, J. L. Dideriksen, S. Conforto, T. DAlessio, G. Severini, J. M. Belda-Lois, L. Z. Popovic, G. Grimaldi, M. Manto, and J. L. Pons, "Multimodal bci-mediated fes suppression of pathological tremor," in *2010 Annual International Conference of the IEEE Engineering in Medicine and Biology*, p. 33373340, IEEE, Aug. 2010.

[64] D. Farina and F. Negro, "Accessing the neural drive to muscle and translation to neurorehabilitation technologies," *IEEE Reviews in Biomedical Engineering*, vol. 5, p. 314, 2012.

[65] M. A. Gorassini, M. E. Knash, P. J. Harvey, D. J. Bennett, and J. F. Yang, "Role of motoneurons in the generation of muscle spasms after spinal cord injury," *Brain*, vol. 127, no. 10, pp. 2247–2258, 2004.

[66] L. M. McPherson and J. P. Dewald, "Abnormal synergies and associated reactions post-hemiparetic stroke reflect muscle activation patterns of brainstem motor pathways," *Frontiers in Neurology*, vol. 13, p. 934670, 10 2022.

[67] E. Martinez-Valdes, F. Negro, C. M. Laine, D. Falla, F. Mayer, and D. Farina, "Tracking motor units longitudinally across experimental sessions with high-density surface electromyography," *Journal of Physiology*, vol. 595, no. 5, pp. 1479–1496, 2017.

APPENDICES

A. *Processing Pipeline*

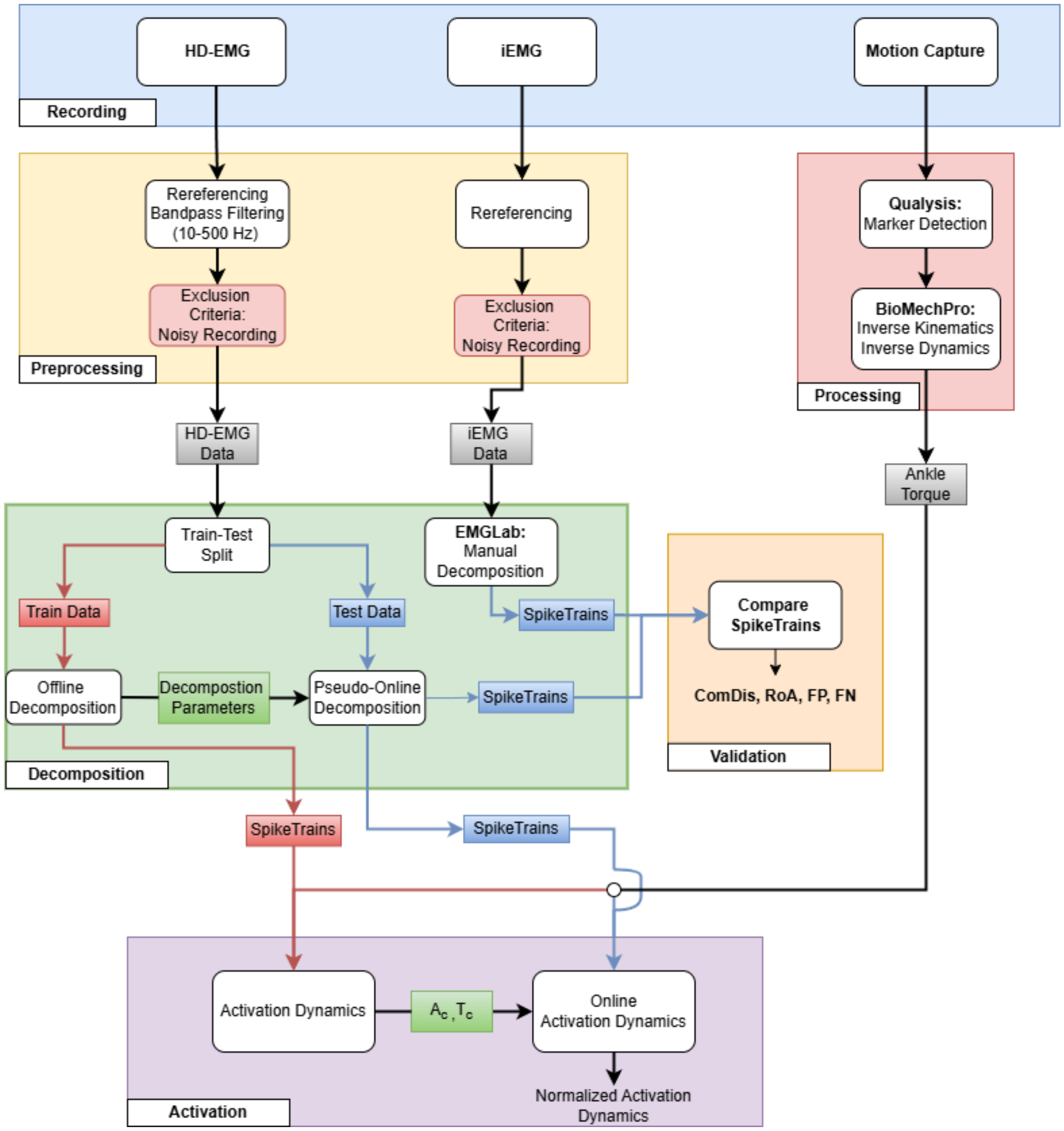

Fig. 9. In the upper blue section, recordings of HD-EMG, iEMG, and motion capture are collected. Once recorded, the iEMG and HD-EMG data undergo preprocessing, as depicted in the yellow "Preprocessing" area. This involves re-referencing and filtering. After preprocessing, both iEMG and HD-EMG data are checked for excessive noise. If no reliable decomposition can be done on either of them, the trial is excluded. Motion capture data follows a separate processing pathway. Marker labeling is performed using Qualisys, and inverse kinematics and dynamics are computed using the BioMechPro toolbox in MATLAB, which uses OpenSim [48]. Following preprocessing, HD-EMG data is divided into a training set (50%) and a test set (50%). Training data usage is indicated by red arrows while testing data usage is marked with blue arrows. In the green "Decomposition" section, the decomposition of both iEMG and HD-EMG data takes place. iEMG data is manually decomposed using EMGLab [8]. Concurrently, offline decomposition is applied to the training data to extract decomposition parameters for pseudo-online decomposition. The spike trains derived from the offline decomposition of training data are also used to initialize amplitude and time constants for activation dynamics (Purple Section). For the decomposition of test data, the data is split into batches to simulate an online setting. The decomposition parameters initialized offline are applied using both static and adaptive approaches, producing spike trains. These spike trains are then compared with iEMG-derived benchmarks to evaluate the performance of different decomposition methods.

The most important MatLab functions for analysis of the data are listed below.

- **Preprocessing HD-EMG**
  - `EMGfilter.m`: Applies bandpass filtering to HD-EMG signals and generates an EMG mask to identify noisy channels.
  - `re_referencing.m`: Rereferences HD-EMG data using an average reference across reliable channels.
- **Preprocessing iEMG**
  - `rereferencing_iEMG.m`: Performs average rereferencing on iEMG data.
  - `main_iEMG.m`: Allows selection of an iEMG file for decomposition and launches EMGLab [8]. Once all motor unit spikes are detected and exported, this function automatically generates spike trains and saves the decomposition results.
- **Offline Decomposition**
  - `decompFastICA_v2.m`: Runs offline decomposition of the HD-EMG training data.
  - `extractOnlineDecompParams.m`: Extracts decomposition parameters from the offline results for subsequent pseudo-online processing.
- **Pseudo-Online Decomposition**
  - `pseudoAdaptDecompOverlap.m`: Segments the test data into batches and runs decomposition using offline-extracted parameters. Depending on the selected settings, it implements either the static or adaptive decomposition approach.
- **Spike Train Comparison**
  - `CompareResults.m`: Compares spike trains obtained from iEMG and HD-EMG decomposition. To address synchronization issues, this script aligns HD-EMG and iEMG data using cross-correlation based on EMG envelopes and spike trains.
- **Synchronization of HD-EMG and Motion Capture Data**
  - `Qual_HDEMG_Sync.m`: Computes the lag between motion capture and HD-EMG data through cross-correlation between torque and EMG envelopes.
  - `Sync_Train_Test_Split.m`: Synchronizes the decomposition results of training and test datasets with ankle torque obtained via inverse dynamics.
- **Activation Dynamics**
  - `ActivationR2.m`: Integrates offline initialization of activation parameters with real-time activation estimation. It uses training spike trains to optimize activation constants A_c and T_c (described in section III-B.2).These parameters are later applied to estimate activation in real time based on spike trains from both static and adaptive decomposition methods.

B. Results Subject 1

In the offline decomposition of subject 1's trials, a total of four common motor units were identified across all trials (see Table III). However, some of these MUs fired in different trials. This is shown in Figure 10, where the iMUAPs from different trials are compared. Specifically, MU1 from the Slow_1 and Normal speed trials correspond to the same motor unit, as the iMUAP shape are alike ($R^2 = 0.9851$). Likewise, MU2 from both Slow_1 and the Slow_2 trials are originated from the same motor unit ($R^2 = 0.9677$). Essentially, this means that only two distinct motor units were identified in this subject. These will be grouped in the following plots to make the comparison easier.

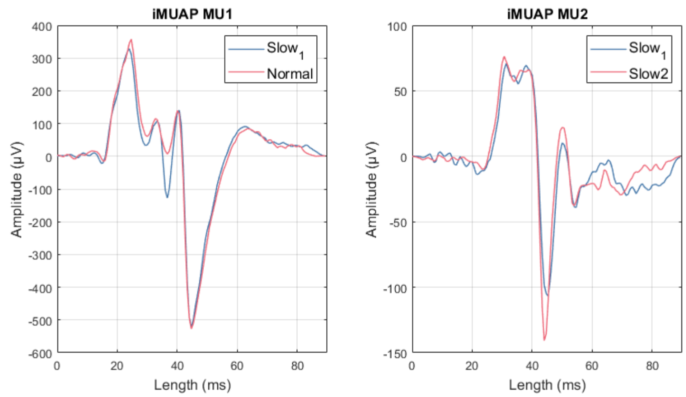

Fig. 10. Grouping of MU based on their iMUAP shape.

1) Using MU filters within a trial: Figure 11 shows the performance when the offline-initialized MU filters were applied to their corresponding test data. In between trials, the quality of some channels of the HD-EMG grid got worse. Therefore, to maximize the decomposition accuracy, a unique mask was used for every trial.

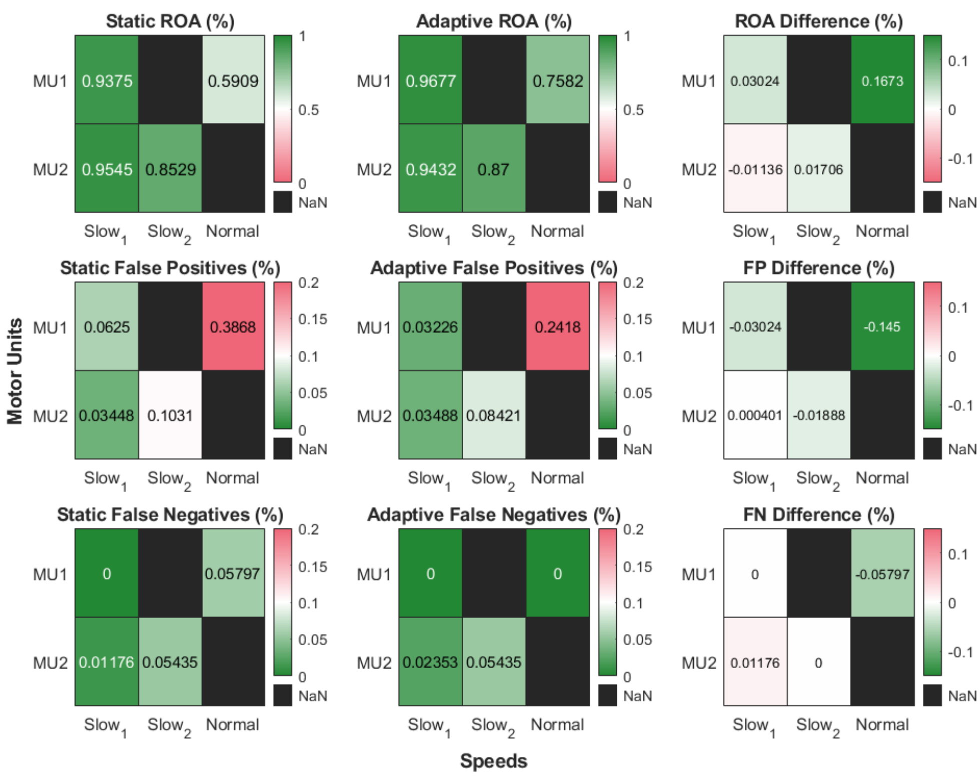

Fig. 11. Results of applying offline-initialized MU filters on their corresponding test data; MU's are grouped based on the NaN values are shown when no common motor units between the HD-EMG and iEMG decomposition were found in static and adaptive decomposition (common discharge $< 50\%$). ** indicates a significant difference (p<0.05).).

2) Using MU filters across conditions/trials: Figures 12 and 13 show the results of applying offline-initialized MU filters to test data of different trials. A common mask was used during the offline procedure for each trial to ensure the resulting MU filters could be applied consistently across different test sets.

At the Slow_1 speed, as depicted in Figure 13, the MU filter for MU2 was not identified in the offline decomposition. This may be due to the use of an incorrect mask, which could introduce noise into the offline estimation of MU filters.

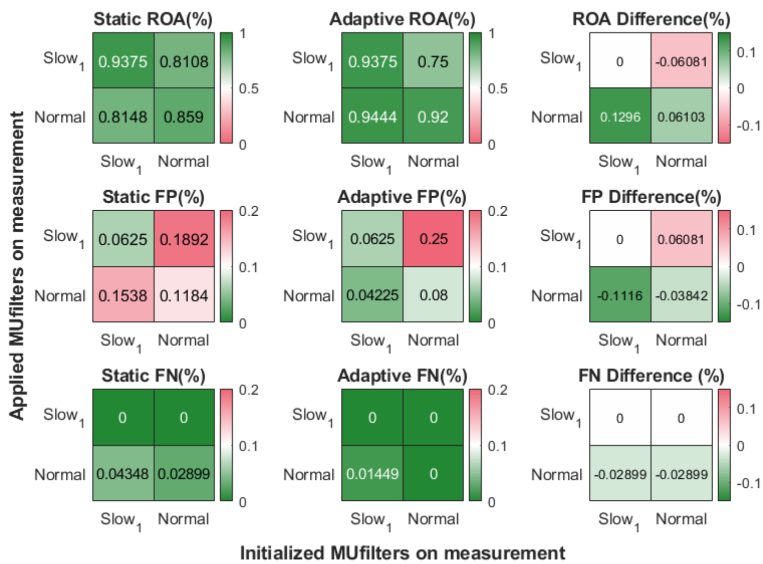

Fig. 12. Cross-comparison of MU1 in Subject 1; The left and middle columns display the RoA, FP, and FN for the static and adaptive decomposition methods, respectively. The right column shows the differences in RoA, FP, and FN between the two approaches (Adaptive - Static), with green indicating better performance for the adaptive method and red indicating better performance for the static method. The diagonal elements of each heatmap reflect the performance of using the offline-initialized MU filters on their corresponding test data.

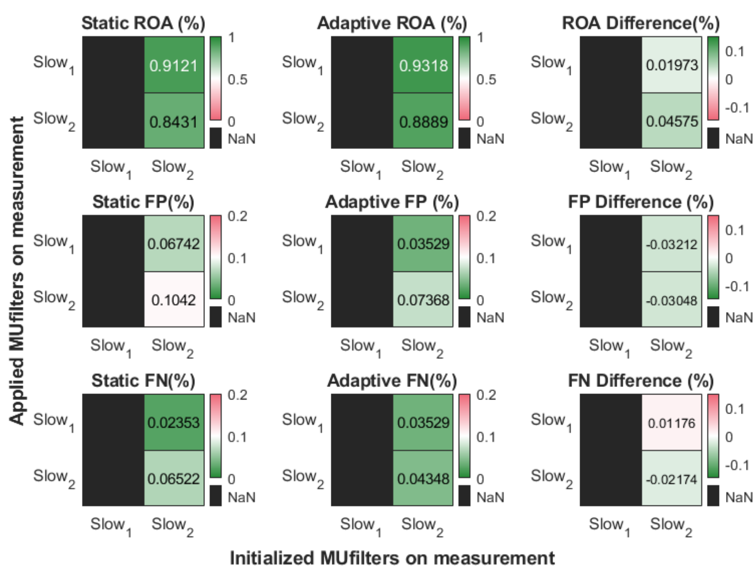

Fig. 13. Cross-comparison of MU2 in Subject 1; The left and middle columns display the RoA, FP, and FN for the static and adaptive decomposition methods, respectively. The right column shows the differences in RoA, FP, and FN between the two approaches (Adaptive - Static), with green indicating better performance for the adaptive method and red indicating better performance for the static method. NaN values represent cases where no common motor units were identified between the HD-EMG and iEMG decomposition (common discharge $< 50\%$). The diagonal elements of each heatmap reflect the performance of using the offline-initialized MU filters on their corresponding test data.

C. Unstable Decomposition

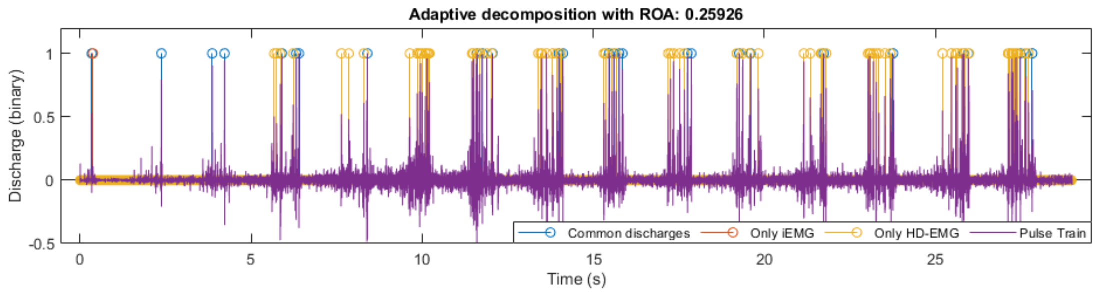

Fig. 14. An example of an unstable adaptive decomposition. The spike train estimate becomes noisy, leading to a significant increase in false positives.